



**UNIVERSIDAD
DE ANTIOQUIA**

**RECENT MORPHOLOGICAL CHANGES IN THE
ATRATO RIVER DELTA: ANALYSIS OF EROSION
AND PROGRADATION TRENDS WITH GOOGLE
EARTH ENGINE (GEE)**

Autor

José Daniel Vélez Castaño

Universidad de Antioquia
Facultad de Ingeniería, Escuela Ambiental
Medellín, Colombia
2020



Recent Morphological Changes in the Atrato River Delta: Analysis of Erosion and
Progradation Trends with Google Earth Engine (GEE)

José Daniel Vélez Castaño

Trabajo de investigación
como requisito para optar al título de:
Magister en Ingeniería Ambiental.

Director.

Julio Eduardo Cañón Barriga
Ingeniero Civil, Ph.D. en Hidrología

Universidad de Antioquia
Facultad de Ingeniería, Escuela Ambiental
Medellín, Colombia
2020.

ACKNOWLEDGMENTS

My hydraulics professor used to tell me that research is not just a process but also a whole lifestyle. It is not only about dedicating two years looking for specific results in a field of knowledge, but also about revolving around questions and ideas, thinking how to answer them and how to build up new questions. According to that point of view, this Master report is the result of a quest that I started many years ago, when I decided that I wanted to challenge my mind with interesting questions that might not have an answer and would create more questions. I want this lifestyle.

There are many people involved in this work both direct and indirect, my family, who endured my absences and gave to me valuable advices. Susana Cadavid who, with patience, supported me and helped me in the weekend closures working on this project.

Special thanks deserve my advisor Julio Cañón, who pushed me forward when I could not find the way or the mood to continue, who gave me valuable advice to get a better job. A large part of successfully completing this master's degree was finding an excellent advisor.

ACKNOWLEDGMENTS	3
ABSTRACT	6
1. INTRODUCTION	7
1.1 Problem statement	7
1.2 Objectives	8
1.2.1 Aim	8
1.2.2 Specific objectives	9
2. THEORETICAL FRAMEWORK	9
2.1 Morphology of deltas	9
2.1.1 Definition of deltas	9
2.1.2 Structure of deltas	9
2.1.3 Classification of deltas	11
2.1.4 Morphometric parameters of deltas	11
2.1.5 Definitions of erosion and progradation	12
2.1.5.1 Erosion	12
2.1.5.2 Progradation	13
2.3 The Atrato River delta	13
2.4 Remote sensing and satellite imagery in the study of deltas	15
2.5 Image segmentation	15
3. MATERIALS AND METHODS	16
3.1 The GEE platform	16
3.2 Satellite data	18
3.3 Data processing	19
3.4 Automatic shoreline delineation	20
4. RESULTS AND DISCUSSION	29
4.1 Automatic shoreline delineation	29
4.2 Accuracy of the automatic shoreline delineation	30
4.4 Automatic tracking of the Delta's shoreline erosion/progradation	32
4.5 Erosion/progradation processes	33
4.5.1 Erosion	33
4.5.2 Progradation	35
4.5.3 Annual and cumulative erosion/progradation	38
4.6 Possible causes of the progradation and erosion fronts	41
5. CONCLUSIONS	43
6. REFERENCES	45

ABSTRACT

The Atrato Delta in Northwestern Colombia has experienced notable geomorphological changes in its shoreline in recent years. We analyze these changes associated with erosion and progradation, using Landsat imagery and Google Earth Engine (GEE) algorithms to identify the processes automatically in an annual basis over the last 33 years (1986 – 2019). We compare the results with manual delineation on the same imagery using ArcGIS, obtaining similar outcomes, although GEE is much more efficient processing large amounts of imagery compared with handmade procedures. We identify with good accuracy trends in erosion and progradation areas along the mouths and sides of the Delta. Our algorithm performs well at delineating the shorelines, although special care must be taken to clean the images from clouds and shadows that may alter the definition of the shoreline. Results show that the Atrato Delta has lost around 10 km² due to erosion and has gained around 18 km² in progradation during the period of assessment. Overall, progradation is the dominant process at the delta's mouths, while erosion is dominant only in areas far from the outflows, which agrees with a river-dominated environment of high sediment loads and is coherent with other studies made in the region. The algorithm in GEE is a versatile tool, appropriate to assess short and long term changes of coastal areas that do not count with land-based information.

1. INTRODUCTION

This document is structured in five sections: 1) introduction, with an overview of the problem statement and the objectives of research; 2) theoretical framework of delta, erosion and progradation concepts, previous studies in the Atrato Delta and the technological advances applied to Earth Observation (EO); 3) materials and methods, presenting the images used, how platform works, the algorithms used and the steps followed to obtain the results; 4) results and discussion, presenting images with automatic shoreline delineation, comparing their accuracy with handmade shoreline delineation, analyzing trends in erosion and progradation; and 5) Conclusions that summarize the main findings of this research.

1.1 Problem statement

In the “Dynamics and Vulnerability of River Delta Systems” meeting held at the University of Colorado in 2007, experts in deltaic environments remarked the importance to conduct studies about vulnerability of deltas based on the following questions (Restrepo, 2008):

1. Which deltas are in erosion, progradation, balance or disintegration stage?
2. In what way river basin and accommodation zone of the delta interact and control the system morphology?
3. In each delta, what are the background conditions of its natural functioning, which serve as a reference to measure the human impact and Global Change?
4. What are the main tensors in each delta (physical and social)?
5. What is the role of the extreme natural events (oceanographic, climatic, hydrological and tectonics) in the recent delta evolution and morphology?

Focused in the first question, the Atrato River delta, in northwestern Colombia, has experienced notable morphological changes in recent years. These changes are the result of the interaction of river flows, ocean waves, tides and human interventions that produce either sediment accumulation or erosion. Evidence of this active reshaping are the increment of sediment loads from 11.3×10^6 tons per year estimated in 2004 (Restrepo and Kjerfve, 2004) to 25×10^6 tons per year in 2011 (Restrepo and Alvarado, 2011). In 2005, the delta had an estimated area of 400 km^2 , which probably grew with the increase of sediment loads along the river (Restrepo and Alvarado, 2011). Figure 1 shows local changes in the geomorphology of the delta (black arrows), where the strong sediment plumes are evident.

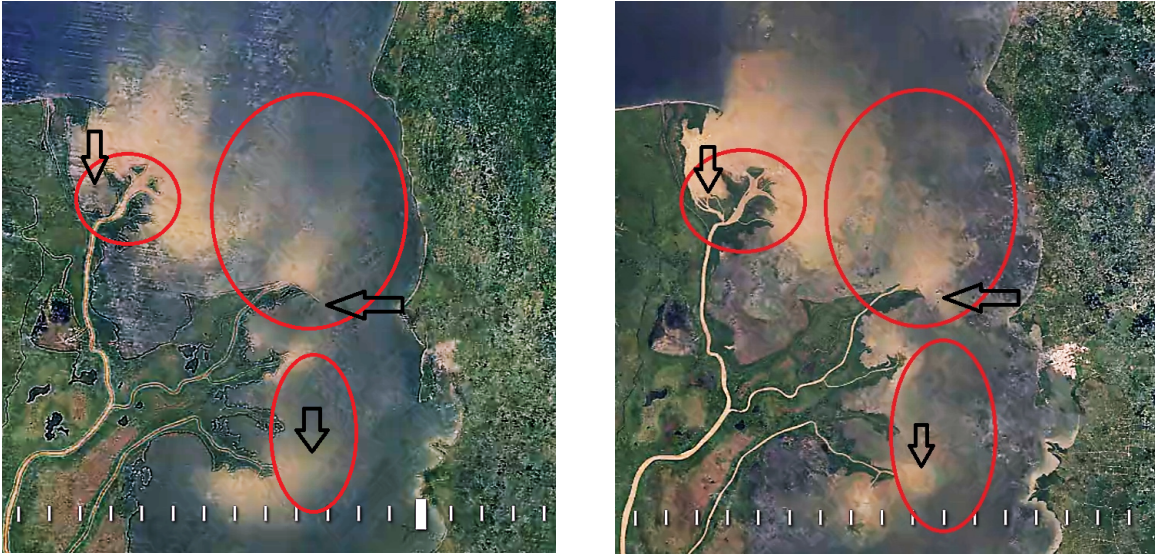


Figure 1. Changes in the Atrato River delta, left: image from 2005, right: image from 2016. Image source: Google Earth Engine, 2018.

These changes are normally determined by hand, overlapping satellite or aerial photographs in chronological order to draw the shorelines, the delta polygon or the river branches (Rangel-Buitrago, 2015; Post, 2011; Hori and Saito, 2007; Nieto, 2004, among others). The manual delineation conventionally performed in Geographic Information Systems (GIS) software is time consuming and cannot be made on a continuous basis, as more images are available.

According with Gorelick *et al.* (2017), Google Earth Engine (GEE) is an online platform designated for researchers and academicians to access, handle and process large satellite datasets. GEE overcomes many of the difficulties arisen from manual delineations by:

- Releasing updated satellite images that can be analyzed automatically.
- Running processes directly in Google servers with the required computing power to analyze large amounts of data in relatively short time.
- Speeding up the image processing.
- Storing the information directly in Google servers (of the order of petabytes).

Based on the above, we want to delineate automatically the Atrato Delta shoreline in GEE to determine annual changes in erosion and progradation areas (and rates) in the last 33 years.

Our hypothesis is that progradation is dominant at the delta mouths due to direct sediment deposition at the river outflows, and that erosion is more common along the sides, where sea waves are dominant.

1.2 Objectives

1.2.1 Aim

This exploratory research aims at identifying progradation and erosion trends in the Atrato Delta shoreline in the last 33 years, based on satellite images.

1.2.2 Specific objectives

To assess the capability of the GEE platform to automatically delineate shorelines in humid areas with high cloudiness.

To track recent morphological changes of erosion and progradation in the Atrato Delta with GEE algorithms and remote sensing images.

2. THEORETICAL FRAMEWORK

2.1 Morphology of deltas

2.1.1 Definition of deltas

Following the definition given by Elliott (1986), we understand a delta as a “...discrete shoreline protuberances formed where rivers enter oceans, semi enclosed seas, lakes or lagoons and supply sediment more rapidly than it can be redistributed by basinal processes”.

The terms “shoreline advances” distinguish deltas from estuaries, in the sense that deltas are regressive/prograding systems and estuaries are transgressive coastal depositional systems (Boyd et al., 1992; Dalrymple et al., 1992). Shorelines architecture and changes are a function of the interactions with the river, ocean waves and tides that exhibit one of the greatest and faster natural forces for landscape transformation (Maselli et al., 2014; Renaud et al., 2013), and recently by man-made activities (Li et al., 2017; Parra & Restrepo, 2014).

The morphology and current configuration of deltas is the response to local factors such as changes in their basin, the ocean currents, climate and isostatic factors (as cited in Restrepo & López, 2008). These morphological changes could occur in very short geological times such as days, months, decades or centuries (Longhitano & Colella, 2007). In some cases, particular events or alterations in some of the factors that contribute to delta formation can exacerbate or minimize these changes.

Deltas extension is difficult to determine due to many existing definitions of delta areas (Restrepo, 2008). Some of these definitions are:

1. Continental area growing towards the sea that have been accumulating sediments since last 6000 years (Amorosi and Milli, 2001).
2. Land belonging to a river valley, beginning in the area where the river divides into its branches (Syvitski and Saito, 2007).
3. River valley area characterized by sea sediments of the Holocene (Kubo et al., 2006).
4. Region with accumulation of continental sediments that have been exposed to fluvial dynamics processes and tidal and wave influences (Overeem et al., 2005).
5. Drained area by the river branches under tidal influence.

Hence, the delta area will depend on the adopted definition.

2.1.2 Structure of deltas

Generally, deltas are composed of subaqueous delta and subaerial delta (Figure 2). The former is characterized by seaward fining of sediments, sand being deposited nearest the river

Morphological changes in deltas may be also driven by many anthropogenic processes such as: deforestation, soil erosion, slope failure, downstream sedimentation, urbanism, farm-animal grazing, agriculture, mining, waterway re-plumbing (reservoirs and dams), diversions, channel levees, floodings, channel deepening, and shoreline alteration among others (Vallejo *et al.*, 2016; Kuenzer *et al.*, 2015; Meyer & Nijhuis, 2013; Dolozi *et al.*, 2011; Kröger *et al.*, 2009).

2.1.3 Classification of deltas

The interplay of fluvial and marine processes produces several types of deltas (Nemec, 1990). According to the delta front regimes, deltas can be classified in high constructional and high destructional. High destructional deltas are marine-dominated and are subdivided in tidal-dominated deltas and wave dominated deltas (Galloway, 1975). Fluvial-dominated deltas are elongated, wave-dominated are cusped, while tide-dominated show estuarine geometry (Hori and Saito, 2007). According to the thickness distribution, deltas are classified as river-dominated, macro tidal dominated, interact riverine-tidal, and wave-dominated (Coleman and Wright, 1975), the Atrato delta can be classified as a high-constructional, river-dominated delta. The Atrato delta shape, close to a bird-foot geometry, formed by prograding, branching distributary channels where the presence of marshes is common.

2.1.4 Morphometric parameters of deltas

The morphometry of river deltas is characterized by a series of morphometric parameters. Mikhailova (2014) proposes four main parameters: delta length through the main branch L (km), delta area F (km²), marginal delta coastline B (km), and the number of branches N outflowing to the marginal coastline. The apex of the delta is the point where the river divides its main channel in distributaries or branches. From that point, L is measured and considered as the beginning of the delta (Syvitski and Saito, 2007).

López and Restrepo (2008) determined the following morphometric parameters: subaerial delta area (A_D), delta plan gradient (D_{grd}), number of branches (C_N), total amplitude of the branches (TC_w), mean amplitude of the branches (C_w), length of shoreline (L_C), delta amplitude (A_m) and subaqueous delta depth (D_{sh}). Other important parameters are progradation and erosion areas and rates. Figure 3 shows some of these morphometric parameters in Atrato River delta.

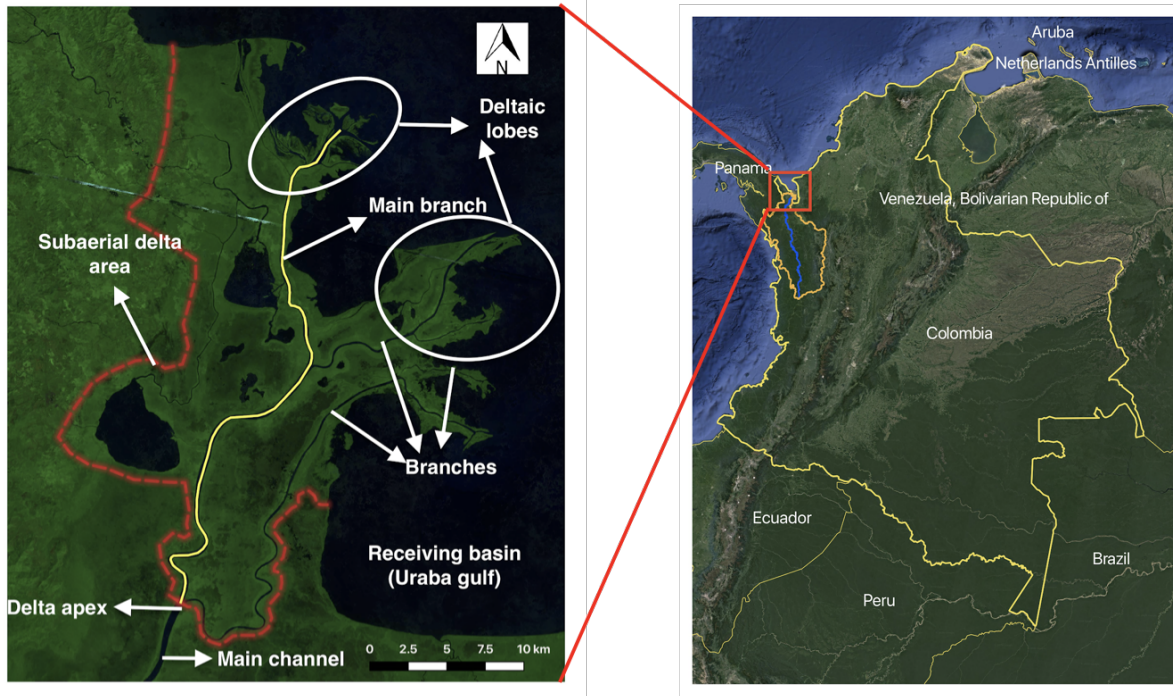


Figure 3. Localization and some morphometric parameters of the Atrato River delta. Image based on Restrepo (2008) (Landsat 8, B7-B5-B3 Natural with atmospheric removal).

2.1.5 Definitions of erosion and progradation

2.1.5.1 Erosion

In a delta, erosion occurs at the shoreline as the wearing of land surfaces that produce losses of beach, shoreline, or dune materials due to natural coastal and human-induced processes (Skaggs & McDonald, 1991), which continually reshapes the shorelines. The natural causes of erosion include the action of wind, waves, and currents. Human actions causing erosion include construction of seawalls, groins, jetties, navigation of inlets and dredging (FEMA, 1997). El Niño and climate changes can exacerbate the natural and human causes of erosion (Haddow *et al.*, 2017).

Both short-term and long-term effects can cause shoreline erosion. The most common type of short-term erosion is from storms; less common are storm surge, overwash, flooding, underflow, navigation inlets, among others. For long-term erosion, sea level rise and decreased sediment supply are the most common. Other long-term erosion processes are deflation, littoral transport loss, sorting of beach sediment, flooding, dams, sand mining, among others (IWR, 2011).

The consequences of erosion range from economical to environmental. The former affects the infrastructure close to the eroding coasts by losing their natural protection. The later includes loss of animal habitats related to economic consequences by fish habitat displacement and landscape modification. An important impact is the loss of tourism, by losing beaches for recreation (Haddow *et al.*, 2017).

Knowledge about the average annual erosion rate is useful to define areas where development should be limited and where special measures should be used for construction (Islam & Ryan, 2016).

2.1.5.2 Progradation

Progradation of a delta is defined as the building of a shoreline or coastline towards the sea (as an increase of beach, delta, or fan fronts) by nearshore deposition of river-borne sediments or by continuous accumulation of beach material thrown up by waves or moved by longshore drifting (Catuneanu, 2002). Progradation occurs due to the interaction of river sediment transport and marine dynamics (Xu, 2006), i.e., sediment transport along the offshore that is important in determining the rates of progradation along the coastal areas (Kaliraj et al., 2013). However, not only hydrodynamic processes take part in progradation: texture and mineralogical characteristics of the beach sediment also intervene in this process.

As in the case of erosion, the causes of progradation can be natural, like storm surge, tsunami, cyclone, waves, tidal, among others; or human, like unregulated mining (Kaliraj, 2013).

Along coastal areas that have experienced progradation (seaward growth), the geomorphic expression of this process, such as consecutive beach ridges, is often used to determine the origin, magnitude, orientation, and chronology of ridge sets or individual ridges (Buynevich et al., 2009). However, the shoreline of a river delta does not prograde uniformly, but migrates only where active channels act as local sediment sources. In fact, mouth-bar deposition and channel bifurcation are fundamental to the progradation process (Jerolmack, 2009).

For both, erosion and progradation processes, multitemporal satellite imagery have been used to detect periodical changes along the shoreline, as they have proved to be as accurate as traditional methods (Jayakumar & Malarvannan, 2016).

2.3 The Atrato River delta

The Atrato River delta is located in the Northwest corner of Colombia, mainly in the department of Antioquia, with some of its channels in the border with department of Chocó, approximately between $N7^{\circ} 50''$ - $N8^{\circ} 30''$ and $W76^{\circ}45''$ – $W77^{\circ} 00''$. The river flows into the Caribbean sea, on the western flank of the Urabá gulf, after traveling northward through a dense and rainy forest from the South of Chocó (Figure 3), that has been affected mainly by anthropogenic activities such as mining, deforestation and agriculture (UPME, 2017; Morita et al., 2017). In this forest, illegal armed groups are present, therefore many of the above activities are difficult to control (Syvitski & Kettner, 2018).

This is one of the rainiest regions of the world with a mean precipitation between 2.500 and 3.000 mm/yr and an average temperature of $33.8^{\circ}C$ (IDEAM, 2018), which explain the cloudiness and humidity that affect observations from satellite imagery. The Delta is located in the Urabá Gulf, where the climate is milder than in the basin, showing a low rainy season from December to April and a high rainy season from May to November.

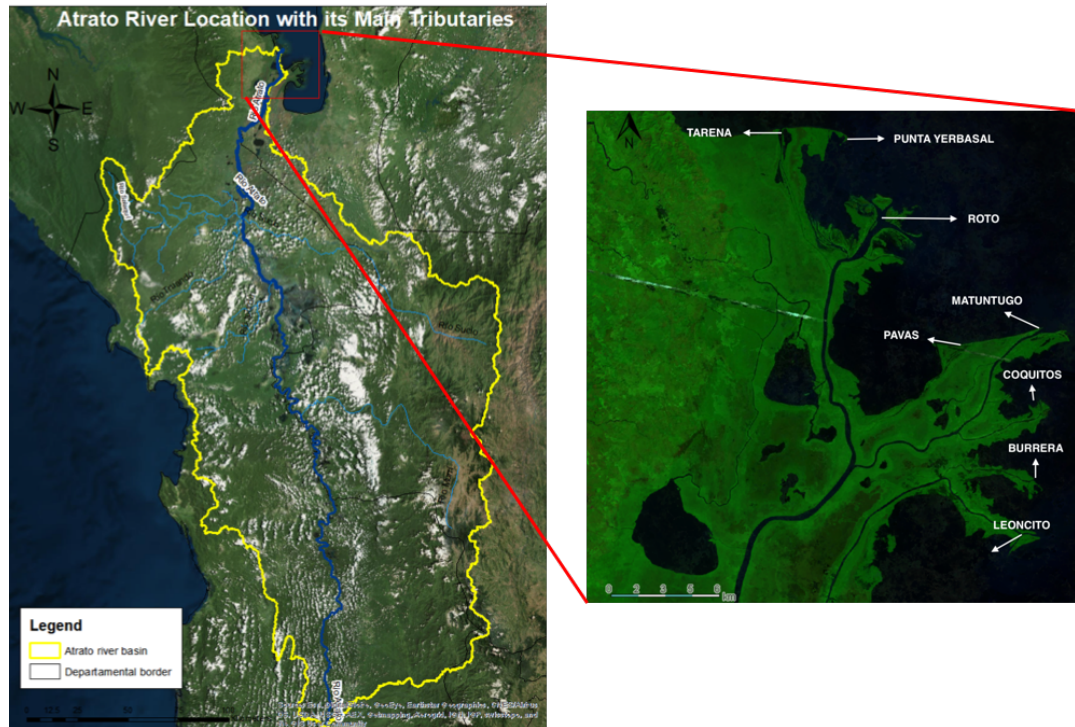


Figure 4. Atrato River basin (in yellow), the delta is the study area (right) and its outflows.

The Delta harbors vast extensions of wetlands and mangroves, which have an important ecological and hydrological value for the ecosystem and people (Post, 2011; Thomas *et al.*, 2007).

The Atrato River delta is a branched system (Escobar, 2011; Post, 2011), reported seven main outflows into the sea: Tarena, El Roto, Pavas, Matuntugo, Coquitos, Burrera and Leoncito (Figure 4), pointing out that only three branches were used for small scale navigation, due to its proximity to Turbo. The outflows are dynamic: as some of them close, new ones open.

The delta lies in an extensive fluvial - lacustrine and alluvial setting of Quaternary and recent deposits. The shoreline geomorphology is determined by the tectonic activity and by the fluvial and marine contributions, which shape this area as a sectorized erosive and cumulative system. The Atrato Delta harbors geoforms related to vegetated-type intertidal planes, flow-marine plains, flood zones and beaches (Blanco, 2016; Posada & Pineda, 2008; Thomas *et al.*, 2007).

One of the most influential factors in the sedimentary dynamics of the delta is the filling of bays with sediment through openings associated with the activity of the mouths of the Atrato, especially during flooding episodes (Vann & Vannl, 1959). This could be a result of the increase of sediment loads from from 11.3×10^6 tons/year in 2004 (Restrepo and Kjerfve, 2004) to 25×10^6 tons/year in 2011 (Restrepo and Alvarado, 2011).

The basin is mainly composed of conserved lands and forest protected by national laws. There are zones that allow practices such as fishing and hunting, and other zones where agriculture, forestry, mining and cattle raising activities coexist. These activities have been expanding, sometimes in an uncontrolled way, changing the land cover and causing an

increase in the sediment loads that reach the Delta and modify its morphology (Abbott *et al.*, 2017; Mateos-Molina *et al.*, 2015; Arroyave-Rincon *et al.*, 2012; Blanco-Libreros *et al.*, 2012; Cuesta & Ramírez, 2009; Restrepo & Restrepo, 2005).

Likewise, the Atrato River delta and its tributaries experience changes due to natural and anthropogenic processes (Vann & Vannl, 1959; Díaz, 2007). The sediment load transported by the river, for instance, increased from an estimated 11.3×10^6 tons/year in 2004 (Restrepo and Kjerfve, 2004) to 25×10^6 tons/year in 2011 (Restrepo and Alvarado, 2011). Similarly the measurements of water discharges in the delta mouths showed values varying from 4138 to 5017 m³/s between 2010 and 2011 (Escobar *et al.*, 2015). This increase has probably been not only due to natural fluctuations, but also likely reinforced by human activities.

The Atrato River flows through a dense, humid and cloudy forest and is the main (almost unique) access and trade route to human settlements in the area since pre Columbian times (Libreros *et al.*, 2013; Thomas *et. al.*, 2007). Almost all settlements are located over riverbanks and depend on the river regimes for their survival. The Delta also nurture a vast area of wetlands (Post, 2011) and mangroves that depend on the Delta's dynamic (Blanco-Libreros, 2016).

2.4 Remote sensing and satellite imagery in the study of deltas

Satellite images have been widely used to monitor deltas due to their capacity to take periodic images in several spatial and radiometric resolutions. These characteristics have allowed to store large collections of multispectral imaging, ranging from coarse to moderate spatial and temporal resolution and including some private commercial satellites of high resolution. Satellite imagery have been used to determine land changes in agriculture, forestry, hydrology, land planning, etc. (Viaña-Borja and Ortega-Sánchez, 2019).

For example, Dang *et al.* (2018) used 59 Landsat images with a maximum of 30% of cloud coverage to study suspended sediment dynamics in the Mekong floodplains, this research shows a significant correlation between the composite reflectance band and measured SSC show the feasibility of using satellite imagery in sediment monitoring, but validation is still necessary.

Fan *et al.* (2017), used 285 images from Landsat mission standard Level 1 Terrain-corrected (L1T), from 2002 to 2015 with cover cloud up to 30% to find a more suitable delta shoreline indicator based on intertidal slope and to quantify seasonal shoreline changes.

A combination of tools to take images can be used to track Earth surface changes as used by Hakkou *et al.* (2018), who used a combination of aerial photographs and satellite imagery to assess the shoreline evolution in long-term. The images showed to be a useful tool for long-term monitoring and assessment of the anthropogenic-morphodynamic evolution of Kenitra coast.

2.5 Image segmentation

Image segmentation is the process of partitioning an image into meaningful regions or objects, grouping in segments that jointly enclose the image or a collection of contours taken out from the image (Nadipally, 2019). Their applications range from locate tumors, measure

tissue volume, study of anatomical structure to locate objects in satellite images (Vala and Baxi, 2013).

The methods for segmenting images are of two categories: edge based segmentation and region based segmentation. The former, uses discontinuities of the image pixels intensities and considers them as a border, the result is a binary image. The latter partitioning an image into regions that are similar according to a set of predefined criteria the result is an image segmented into areas of connected pixels with similar color, intensity and/or texture (Vala and Baxi, 2013).

Most known methods in edge-based segmentation are gray histogram based and gradient based method. In this method, all pixels of an image are taken into consideration to figure the histogram, and the valleys and peaks in the histogram are utilized for establishing the clusters in an image (Nadipally, 2019).

In region based segmentation methods the most known are thresholding, region growing and region splitting (Vala and Baxi, 2013). Thresholding method is an important technique; the basic idea is to select an optimal gray-level value (threshold) for separating objects of interest in an image (Nadipally, 2019). Thresholding creates binary images from grey-level ones by turning all pixels below some threshold to zero and all pixels about that threshold to one. Is very useful in images with strong changes in pixel distribution (Donchyts *et al.*, 2016).

All the image segmentation methods assume that: the intensity values are different in different regions and within each region representing the corresponding object in a scene, he intensity values are similar.

The expression that resume thresholding method is:

$$if f(x, y) < T then f(x, y) = 0 else f(x, y) = 1$$

The expression means that any value above a threshold T will be taken a 0 and any value below T will be taken as 1 , which gives a binary image.

Recently, deep learning become a useful tool to image classification, detection, segmentation, among others image processing. This method uses Convolutional Neural Network (CNN) or any of its variations and can address image segmentation from multiples strategies (see Liu *et al.*, 2015; Vilariño *et al.*, 1998; Milletari *et al.*, 2016; Chen *et al.*, 2016; Bao and Chung, 2018)

3. MATERIALS AND METHODS

3.1 The GEE platform

To perform the images analysis and processing, we used Google Earth Engine platform (GEE), a cloud-based platform for planetary-scale geospatial analysis, accessed and controlled through an Internet-accessible application programming interface (API) and an associated web-based interactive development environment (IDE) (Gorelick *et al.*, 2017), to observe morphological changes in the Delta.

This platform contains an extensive and constantly growing data catalog with petabyte-scale archive of publicly available remotely sensed imagery and other data like features (vectors). It has a computational infrastructure optimized for parallel processing of geospatial data (Gorelick *et al.*, 2017).

The platform has an interface named code editor, an online Integrated Development Environment (IDE) for rapid prototyping and visualization of complex spatial analyses, with a variety of features. In this interface, we can upload, import and visualize the imagery that we need to our purposes without caring for storage capacities, further do advanced calculations, statistical and geostatistical analysis and geospatial analysis (Figure 5). A little drawback of GEE is that it only allows running the entire code, not specific sections of it, which could be frustrating, especially when trying to debug long algorithms.

In addition to code editor, GEE has others way to interact with the platform: explorer and client libraries. The first one is a interface that allows anyone to visualize the data. Users can also import data, run simple analyses, save, and export the results. The second provide JavaScript and Python wrapper functions for the Earth Engine API.

An important feature of GEE is the use of *MapReduce* architecture for parallel processing, this allows handling large amounts of location based information attached to Google searches as well as geographical imagery (e.g. satellite images) and features (e.g., road segments and landmarks). With this architecture, GEE does complex calculations by using “batch” processing data, e.g. dividing the information (like image collections) into separate chunks (Gorelick *et al.*, 2017).

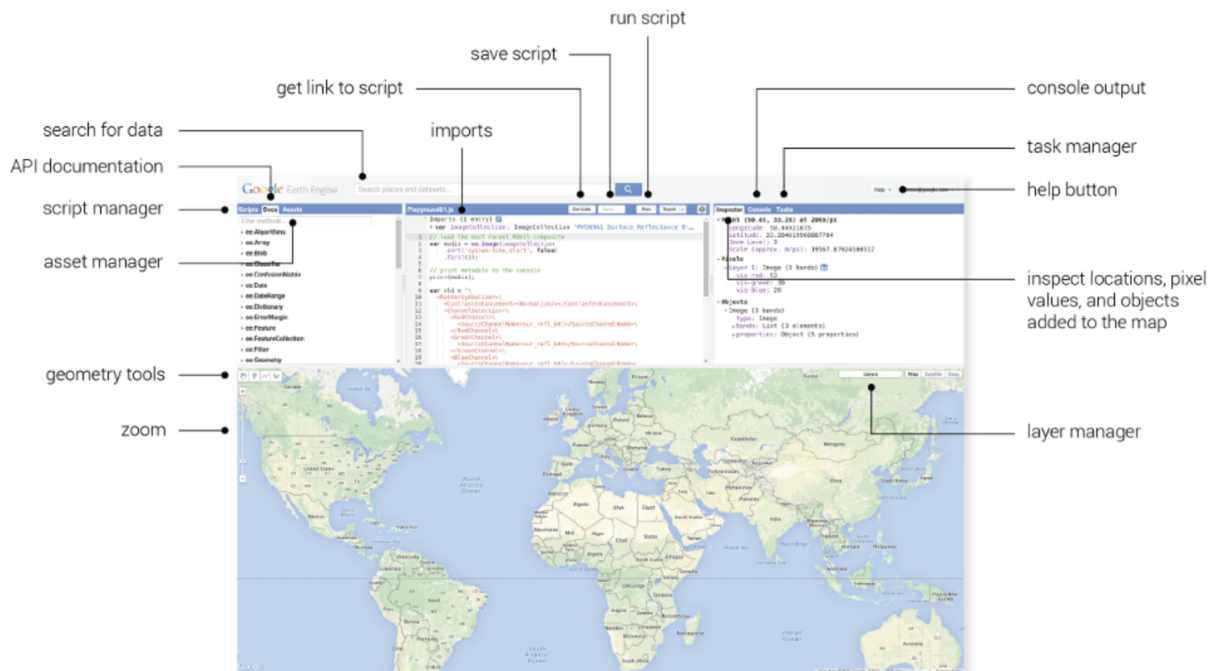


Figure 5. GEE platform interface. Reproduced from: <https://earthengine.google.com/platform/>

GEE has several predefined algorithms, called methods, to conduct processes that avoid us from writing large scripts. These methods are designed specifically for each imagery collections.

Compared with other GIS softwares, GEE is free (previous subscription) and centralizes petabytes of satellite imagery (Alonso *et al.*, 2016) such as MODIS, LandSat and Sentinel. The images can be accessed easily at different levels of processing (i.e., calibrated at sensor radiance or Top Of Atmosphere (TOA), reflectance or atmospherically corrected Surface Reflectance (SR)), which facilitate the timely use and manipulation of images.

GEE is the platform used to write the algorithm that allowed us to process the satellite imagery, sort it chronologically, make images composites, mosaicking, automatically delineate the shoreline at delta and its surroundings and calculate progradation and erosion areas. GEE allowed us also to validate the results of the algorithm comparing them with handmade delineation in a GIS software.

3.2 Satellite data

To track the delta changes we used imagery from Landsat 5, 7 and 8 Tier 1 raw scenes. These scenes include Level-1 Precision Terrain (L1TP) processed data that have well-characterized radiometry and are inter-calibrated across the different Landsat sensors, with a revisit time of 16 days (USGS, 2019).

Landsat program is the world's longest continuously acquired collection of space-based land remote sensing data (Alonso *et al.*, 2016), which sensors record several spectral bands at spatial resolutions between 15 and 120 m. We chose Landsat images due to their spatial resolution that is adequate to tracking geomorphological changes in small distances and for their long records (Table 1). For our purposes, we used spectral bands at 30 m of spatial resolution. We processed images recorded during the dry season (November to April) when cloudiness is relatively low. We selected all the available images within the dry season between 1985 and 2019, for a total of 194 images in the path-row grid 10-54 and 10-55 in Landsat world reference grid (WRS-2) (USGS, 2019), where the Atrato River delta is located (Figure 6).

Table 1. Number of images Landsat after filtering by date and boundary

MISSION	RANGE DATES ACQUISITION		PATH	ROW	NUMBER OF IMAGES
	START	END			
Landsat 8	2013/04/01	2019/04/28	10	54	65
			10	55	50
			Subtotal		115
Landsat 7	1999/11/07	2003/03/23	10	54	22
			10	55	26
			Subtotal		48
Landsat 5	1985/03/04	2011/03/12	10	55	9
			10	54	22

Subtotal	31
TOTAL	194

The Landsat images were obtained import them from the GEE platform to code editor, performing a search in a “search for data” bar in the code editor interface. Landsat images are imported as an “*image collection*” which is a stack or time series of images with properties that allow filtering according with a particular interest like date, path-row, cloud cover percentage among others.



Figure 6. Paths and rows where the Atrato River Delta is located.

3.3 Data processing

We analyzed Landsat 5, 7 and 8 raw scenes at Level-1 Precision Terrain (L1TP). To reduce the incidence of cloudiness we chose mostly images from the dry season (November to April). We filtered the scenes by boundary and dates to limit the number of results. As a boundary, we use the Atrato River basin polygon (see Figure 4) and as dates, we chose images between November and April from 1985 to 2019. Using these filters, we reduce the collection from more than 5000 images to 194 (Table 1).

With these images we created a composite, using `ee.Algorithms.Landsat.simpleComposite()`, which selects a subset of scenes at each location, converts to TOA reflectance, applies the simple cloud score and takes the median of the least cloudy pixels (Google Earth Engine,

2018). Cloud score is the size of the range of cloud scores to accept per pixel, the range of values are between 0% and 100%, being 0% an image with no clouds in its pixels and 100% pixels with total cloud cover. Our cloud score value is 25% that means that we accept images up to 25% of cloud cover.

Figure 7 illustrates the processes that we followed to obtain the image composition for the study period.

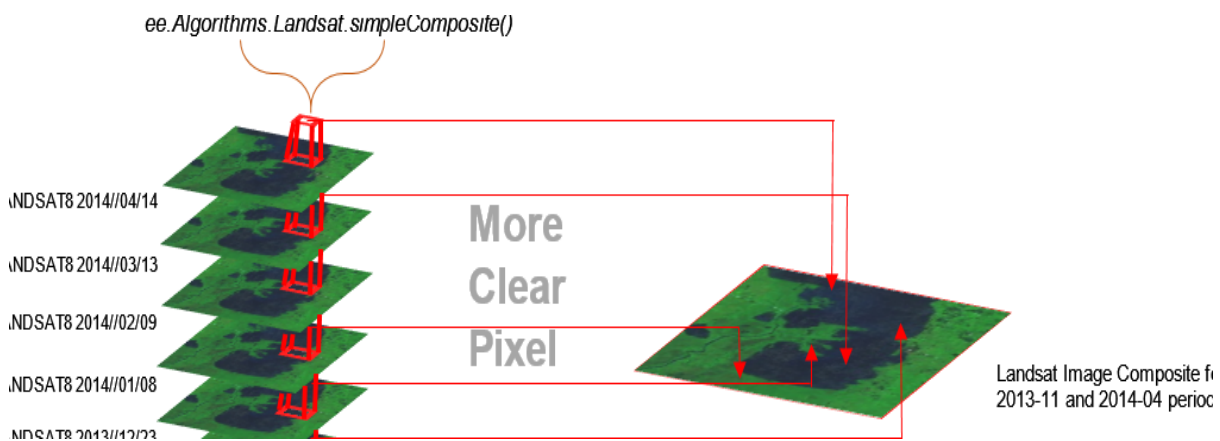


Figure 7. Process followed to get an image composite

With the composite images, we perform a mosaicking process to Landsat 5, 7 and, 8. Mosaicking is applied since each path-row image only covers part of the study area, hence we must assembled mosaics of two images (images path-row 10-54 and 10-55) to produce a spatially continuous image (Google Earth Engine, 2019).

After mosaicking, we obtained 17 images, one image per period, covering from 1985 to 2019 (there were some years where we did not find images available or images with low quality: 1987, 1988, 1993 to 1996, 2004 to 2009 and 2012). We reviewed further the image composites obtained and applied a filter to decide if the image was suitable for analysis (the filter consisted in observing the cleanliness of the scene).

With the 17 images, we created a list of images sort them chronologically, to facilitate apply year to year the followed processing steps

3.4 Automatic shoreline delineation

We set Landsat 5 1985 - 1986 (We discarded Landsat 5 1984 - 1985 due their cloudiness over the area of interest), as a baseline to compare the evolution (progradation or erosion) of the delta. To observe these changes we delineated the shoreline of all processed images and compared them. Normally, the manual delineation in GIS software requires the creation and edition of a vector layer in each image. This task is tedious and time consuming for many images.

We used image segmentation techniques to automate the process of delineating the shoreline of the delta area in each image. We selected the Otsu's method (Otsu, 1979) due to its simplicity and effectiveness (Vala and Baxi, 2013).

Otsu method is a global thresholding method of the region based segmentation image type. This method depend on the gray value of the pixel, without considering the pixel's spatial neighborhood, hence it requires the computation of a grey level histogram. The Otsu method works well when there is marked visible bimodal peaks and valleys in the histogram, but when the histogram do not present these behaviors the method could fail.

In our case, Otsu's method automatically calculate an optimal threshold from an image that contains two classes of pixels (water and land), following bimodal histograms (Otsu, 1979).

We summarize the mathematical principles of the Otsu's method below (based on Otsu, 1979, and Wang, 2007):

Otsu's method is adequate to perform image partition for two classes C_0 and C_1 at gray level t such that:

$$C_0 = \{0,1,2,3,\dots,t\} \text{ and } C_1 = \{t+1,t+2,t+3,\dots,L-1\}$$

where L is the total number of grey levels of the image. Let the number of pixels at the i th gray level be n_i and n be the total number of pixels in a given image. The probability of occurrence of grey level i is defined as:

$$p_i = \frac{n_i}{n}$$

C_0 and C_1 normally correspond to the object of interest and the background. The probabilities of the two classes are ω_0 and ω_1 :

$$\omega_0 = \sum_{i=0}^t p_i \text{ and } \omega_1 = \sum_{i=t+1}^{L-1} p_i$$

Thus, the means of the two classes can be computed as:

$$\mu_0(t) = \sum_{i=0}^t \frac{ip_i}{\omega_0(t)\mu_1(t)} \text{ and } \mu_1(t) = \sum_{i=t+1}^{L-1} \frac{ip_i}{\omega_1(t)}$$

Let σ_B^2 and σ_T^2 be the between-class variance and total variance respectively. An optimal threshold t^* can be obtained by maximizing the between-class variance:

$$t^* = Arg \left\{ \max_{0 \leq i \leq L-1} \left(\frac{\sigma_B^2}{\sigma_T^2} \right) \right\}$$

where the between-class variance σ_B^2 and total variance σ_T^2 are defined as:

$$\sigma_B^2 = \omega_0(\mu_0 - \mu_T)^2 + \omega_1(\mu_1 - \mu_T)^2 \text{ and } \sigma_T^2 = \sum_{i=0}^{L-1} (i - \mu_T)^2$$

The total mean of the whole image μ_T is defined as:

$$\mu_T = \sum_{i=0}^{L-1} ip_i$$

In our study, we applied Otsu’s method to one single band to calculate the threshold. We chose the NIR (Near InfraRed) band since it discriminates well between water (highly absorptive) and land, particularly vegetated land (highly reflective).

We adapted the algorithm implemented by Donchyts *et al.*(2016) in which the authors searched only over the thresholds represented by the bins in a histogram. In this algorithm, the objective is to find the threshold that maximizes interclass variance defined as BSS/p (Donchyts *et al.*, 2016), where p is the number of classes and BSS (Between Sum of Square) is given by:

$$BSS = \sum_{k=1}^p (\underline{DN}_k - \underline{DN})^2$$

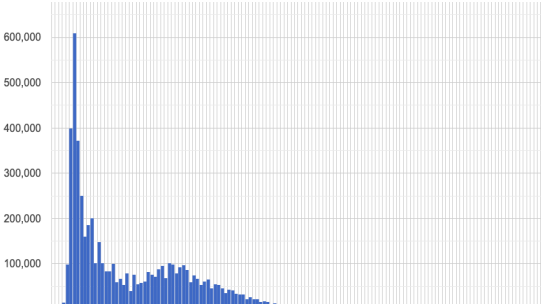
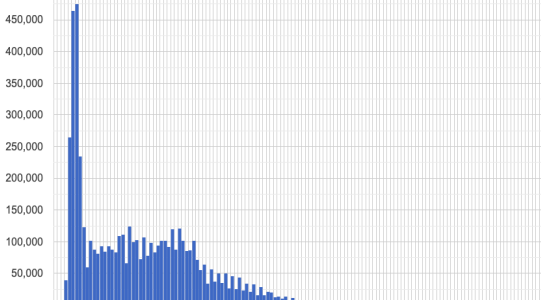
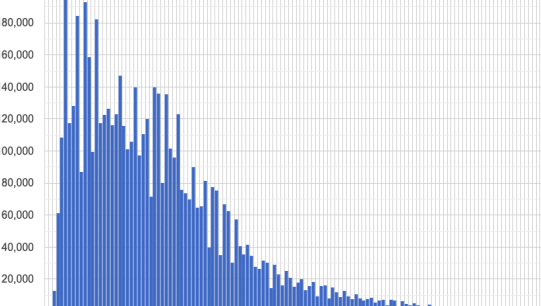
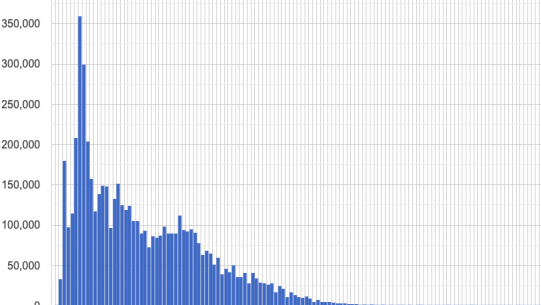
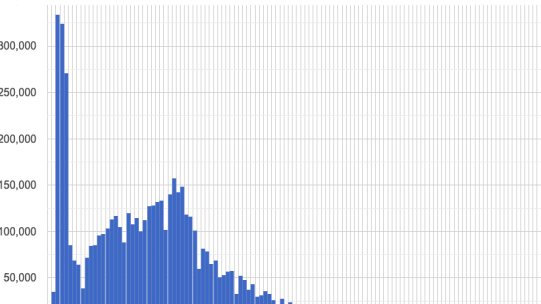
For our two classes (land and water) $p = 2$. DN is the digital number of the NIR band, \underline{DN}_k is the mean digital number in class k and \underline{DN} is the mean digital number of the entire dataset. Class k is defined by every DN less than some threshold (Donchyts *et al.*, 2016). We replaced DN with reflectance, since TOA images preserve the bimodal histogram that is the base of the method. Donchyts *et al.* (2016) used this methodology in satellite image analysis to assess the change in surface water at a global scale with GEE.

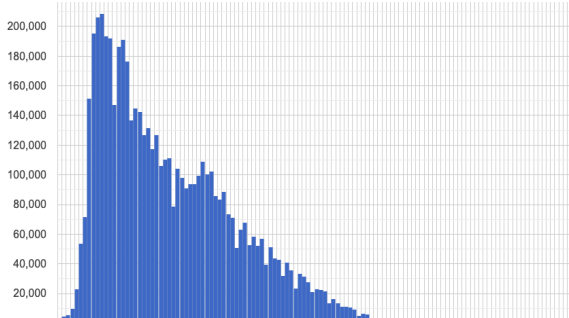
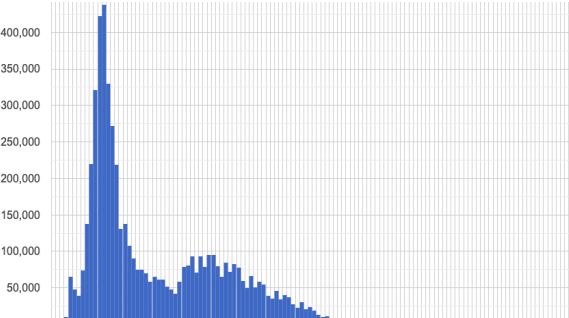
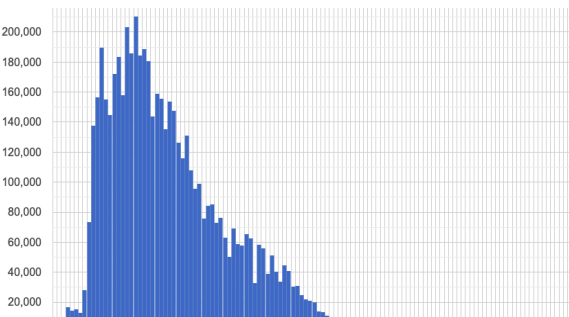
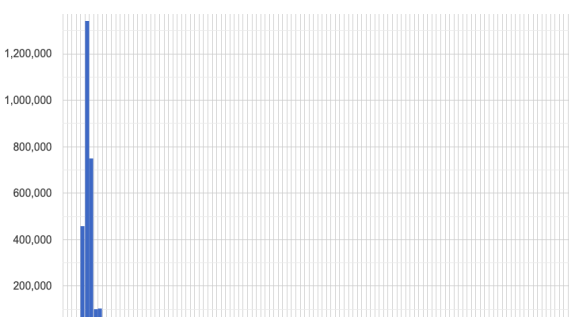

The advantage of such approach is that it only requires a single pass over the data. At each bin of the histogram, we define a class k as the pixels in that bin and lower. Class $k+1$ contains everything else. The algorithm looks at every possible partition of the input data defined by the bins of the histogram, then returns the mean associated with the bin that maximizes the BSS (Donchyts *et al.*, 2016).

Table 2 summarizes the histograms determined to search the threshold and the threshold value can be seen in.

Table 2. Histogram of the images and the threshold for Otsu’s method

HISTOGRAM	THRESHOLD	IMAGE
	0.1704	Landsat 5 1985-1986

HISTOGRAM	THRESHOLD	IMAGE
	0.1319	Landsat 5 1986-1987
	0.16	Landsat 5 1989-1990
	0.1742	Landsat 5 1991-1992
	0.1501	Landsat 5 1997-1998
	0.17374	Landsat 7 1999-2000

HISTOGRAM	THRESHOLD	IMAGE
	0.1532	Landsat 7 2000-2001
	0.1541	Landsat 7 2001-2002
	0.1699	Landsat 7 2002-2003
	0.1684	Landsat 5 2010-2011
	0.1708	Landsat 8 2013-2014

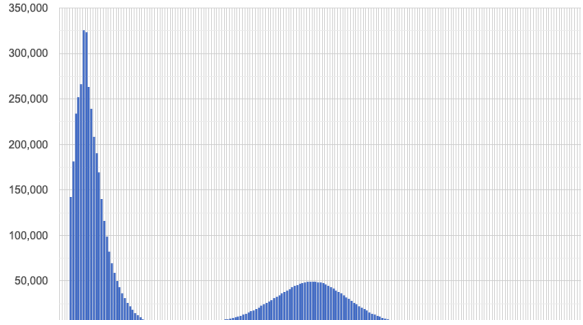
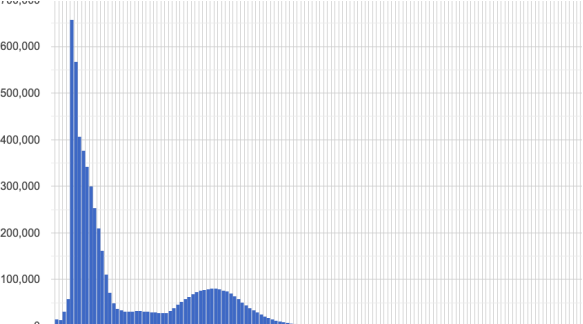
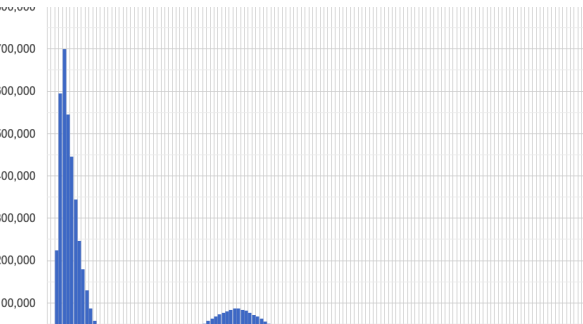
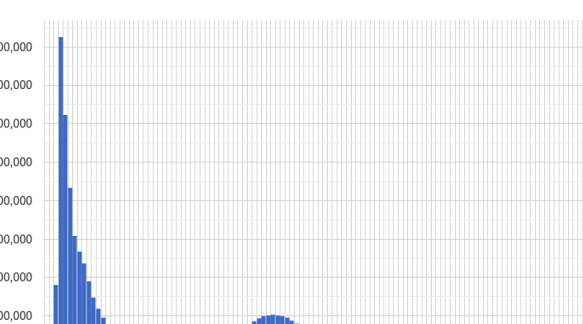
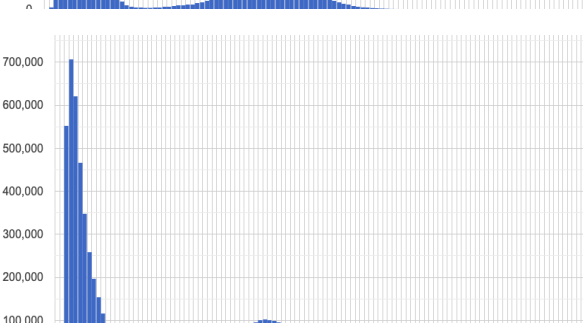
HISTOGRAM	THRESHOLD	IMAGE
	0.1455	Landsat 8 2014-2015
	0.1877	Landsat 8 2015-2016
	0.1568	Landsat 8 2016-2017
	0.15916	Landsat 8 2017-2018
	0.1451	Landsat 8 2018-2019

Table 2 shows that images from Landsat 8 presented well-defined bimodal histogram, which allowed us to take images almost without any noise and near perfect delineation. Landsat 7 and 5 have images where the histogram only shows one peak, so in some areas of the images the delineation was not clear, as we will see in next section.

The application of Otsu's method yields a series of polygons, one per year, in which one side represents the Delta's shoreline (Figure 8) and the other the waterline. We compared the polygons by subtracting one polygon from another, using the *left.subtracting(right)* algorithm, which returns the result of subtracting the right geometry from the left geometry. We obtained the annual erosion and progradation polygons as follows:

$$Polygon_{year\ i}.subtracting(Polygon_{year\ i+1}) = Polygons_{erosion\ year\ i+1}$$

$$Polygon_{year\ i+1}.subtracting(Polygon_{year\ i}) = Polygons_{progradation\ year\ i}$$

In a similar fashion, we obtained the cumulative erosion and progradation at each period (from 1986-1987 to 2018-2019), setting 1986-1987 as a benchmark:

$$Polygon_{1986-1987}.subtracting(Polygon_{period}) = Polygons_{cumulated-erosion-period}$$

$$Polygon_{2018-2019}.subtracting(Polygons_{period}) \\ = Polygons_{cumulated-progradation-period}$$

To classify the rate of erosion/progradation, we chose the hotspots (critical areas) and grouped them in four categories of coastal evolution trend, according with Rangel-Buitrago *et al.* (2015): high erosion (≥ -1.5 m/yr), erosion (-1.5 to -0.2 m/yr), stability (-0.2 to +0.2 m/yr) and progradation ($\geq +0.2$ m/yr).

We applied the above methodology to all images. Figure 9 depicts the flow chart we followed in the process.



Figure 8. Polygon obtained after applied Otsu method, one of its sides is the shoreline of the delta

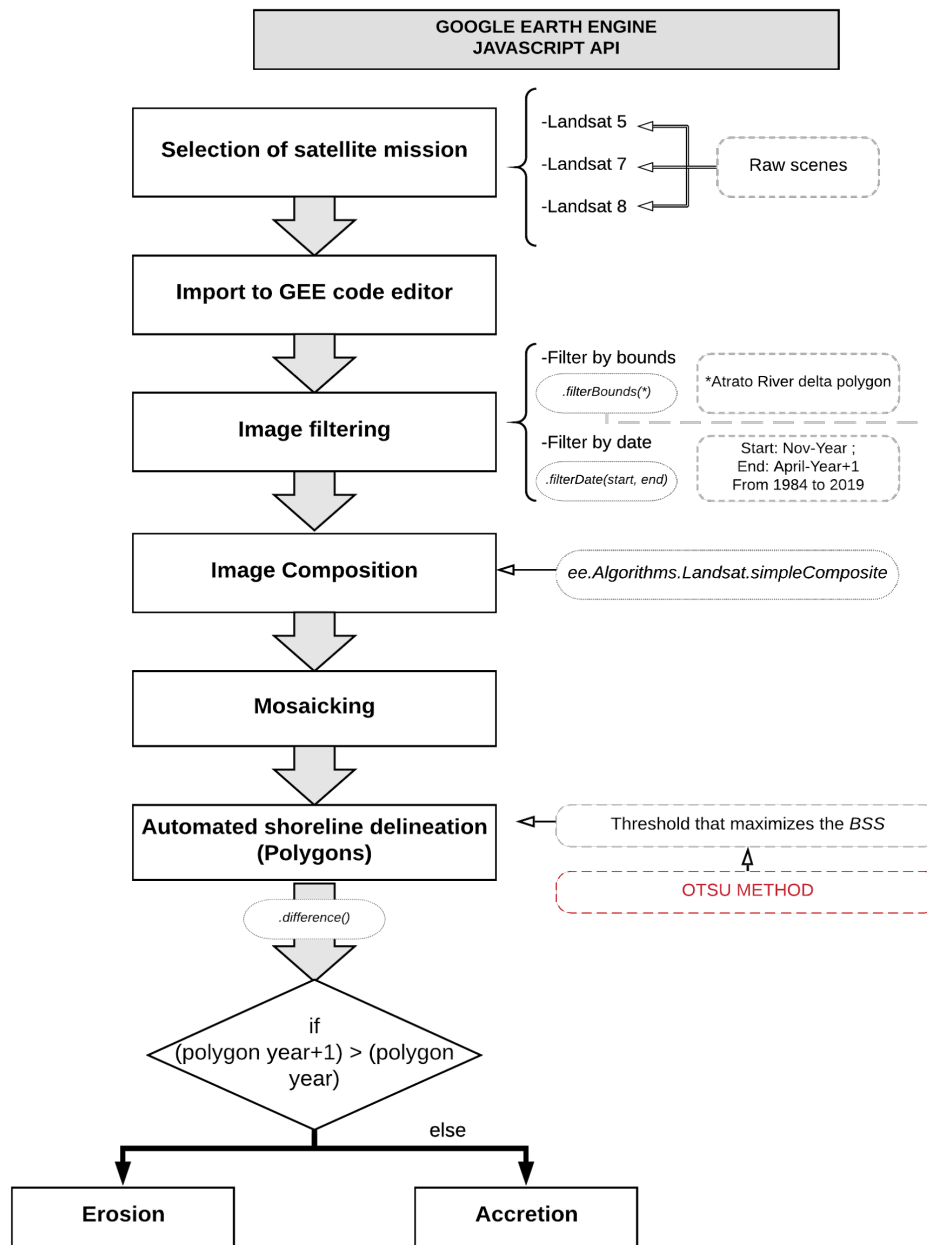


Figure 9. Flow chart depicting the steps implemented in GEE API to obtain the annual shorelines of the Atrato River delta.

4. RESULTS AND DISCUSSION

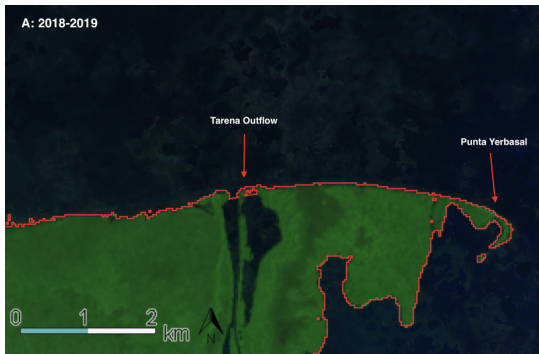
We present the results from three approaches, according with our initial purposes: 1) determine the capacity of GEE to efficiently generate the shorelines; 2) Define the accuracy of the automated shoreline delineation; and 3) Analyze the changes in progradation and erosion observed over the Delta's shoreline based on the comparison of the shorelines in different times.

The amount of images available for area of the delta in each mission decreases from Landsat 8 (115 images) to Landsat 5 (31 images) for the period of interest, which affects the quality of the image composite, since there are fewer images to get clean pixels.

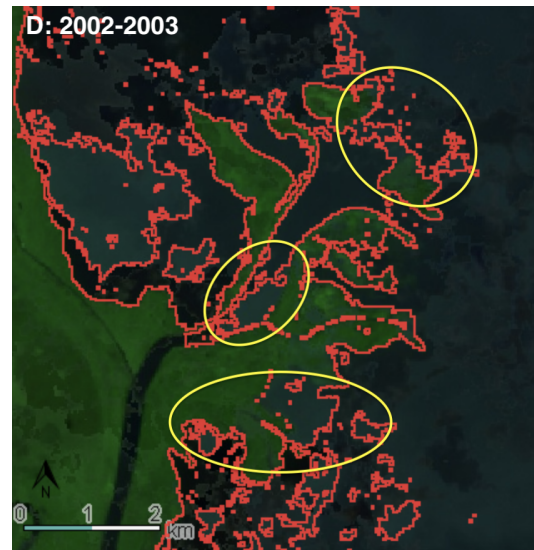
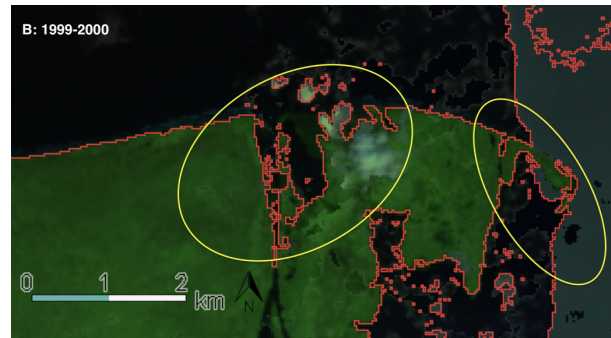
4.1 Automatic shoreline delineation

To analyze if the line obtained from the automatic delineation was a good representation of the delta front, we visually compared between the line and the image for the same period. In Figure 10 we present examples of good automated delineations of the delta frontline compared to poorly automated delineations at different parts of the Delta.

GOOD AUTOMATED DELINEATION



POOR AUTOMATED DELINEATION



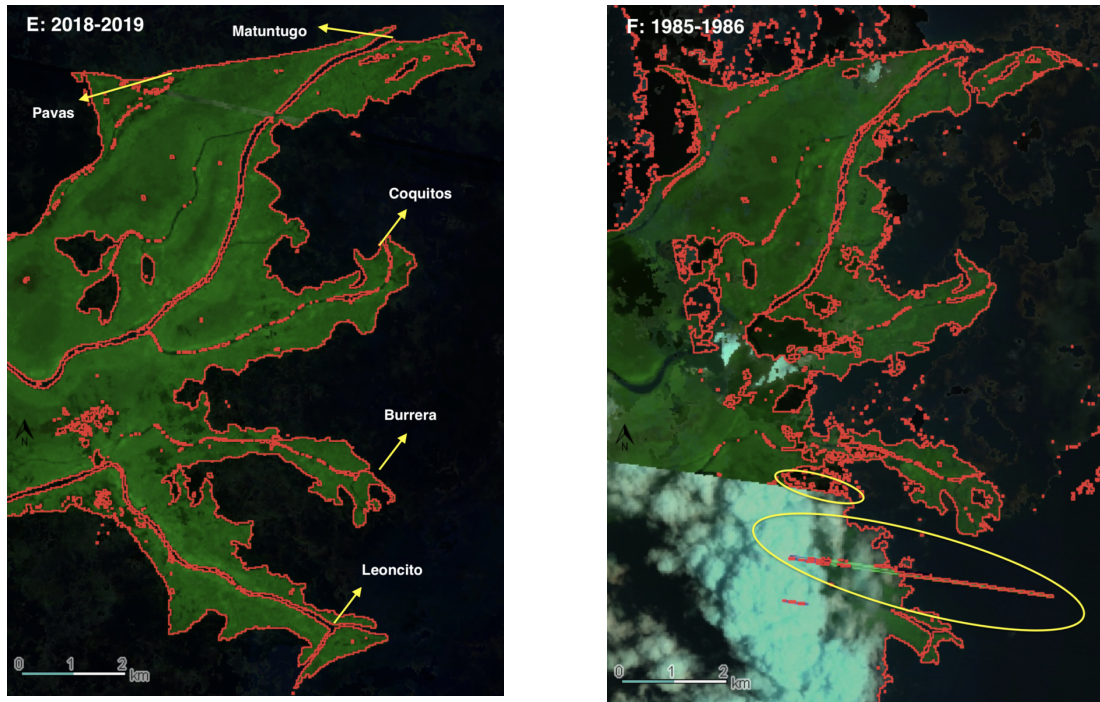


Figure 10. Comparison between good (left) and poor (right) automated delineations of the Atrato River delta shoreline.

Scenes A and B show Tarena outflow area. In this zone, we found five images with some kind of noise but only one was discarded.

Scenes C and D show the geometric configuration of the El Roto outflow and its multiples channels that were a challenge for the algorithm to discern its banks, especially when the lines were relatively close, but, as we see in scene C, the delta frontline was clearly delineated. At El Roto only one image was discarded due to noise.

In scenes E and F, we grouped five outflows in one single image and we found that this area presented the noisiest images at the delta area. Nonetheless, we could conduct the analysis with only one image discarded. 1999-2000 and 1997-1998 images presented a stripe crossing them, caused by the overlapping of edges between path-row 10-54 and 10-55 in the mosaic.

In general, the algorithm was robust and efficient (with only three out of 17 images discarded). The image collection with more restrictions was Landsat 5 due its lower amount of images available to perform an adequate composite. The discarded images belonged to landsat 7, one in 1999-2000 and two in 2001-2002. All landsat 8 images, except 2015-2016, presented high quality and were the images with clearest delineated shoreline, which is coincident with the large number of images available from this mission.

4.2 Accuracy of the automatic shoreline delineation

Our delineation algorithm on GEE can be applied to an area with heterogeneous reflectances (i.e., presence of clouds and shades), but we still need to determine the degree of accuracy within which the shoreline is delimited. Therefore, we visually validate the results by tracing the shoreline by hand for the periods 2001-2002 and 2013-2014, using the high-resolution

composites from Google Earth images (GE) of 2019, and comparing them with our automated traced shorelines on GEE.

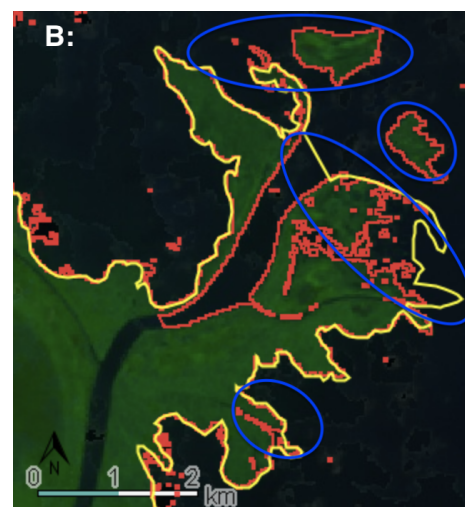
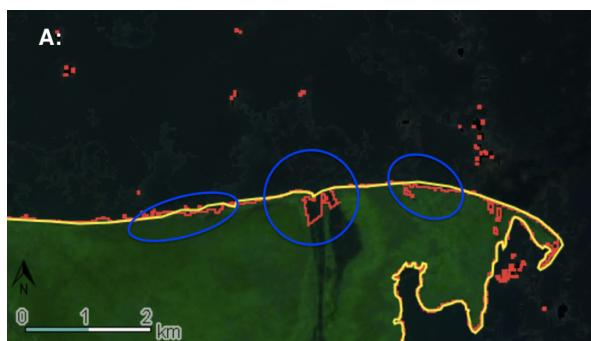
The results confirmed the power of the algorithm to achieve satisfactory delineations with low quality images. It is worth noticing that the satellite images have a 30 m resolution, which causes the observed pixelation of the shoreline.

In almost all the delta, both lines are coincident in its trace in 2001-2002 (Figure 11). GEE was even able to identify small islands and channels (Figure 11). For instance, in image D it detects an island formation very close to the shoreline and in image C it detected two little channels.

The islands formed within the delta are important because they are the result of the interaction between the river's flows, sediment loads and the ocean hydrodynamic. The manual delineation omitted the island but the algorithm recognizes it, as shown the blue circle in image B of Figure 11.

As we can see in Figure 10B the image is not clean enough and the algorithm interpreted the change in the image contrast as the shorelines giving as a result a false shoreline, this means that if the image present strong contrast the algorithm could fail. In our case, the algorithm delineated the delta shoreline with high precision in all years and therefore, we were able to track changes in the delta shoreline.

The match between shorelines delineated by hand and with GEE for the period 2013-2014 was even better, as can be seen in Figure 11, images C and D. This was the result of good composites obtained from a large number of images available in Landsat 8.



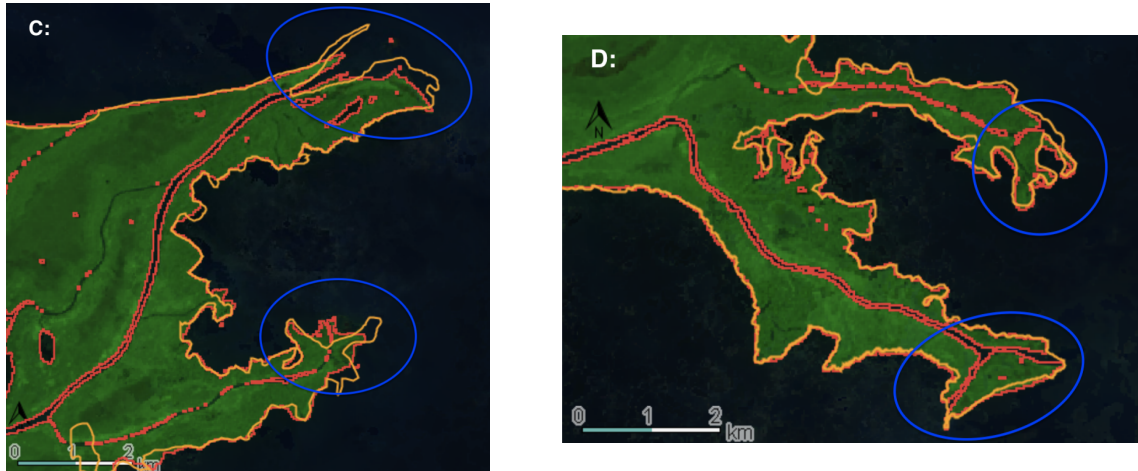


Figure 11. Automated shoreline drawn with GEE (in red) compare to shoreline drawn by hand (in yellow) for 2001-2002 (A and B scenes) and for 2013-2014 (C and D scenes).

Images C and D in Figure 11 showed some discrepancy between the two lines caused by clouds and shadows that we confused with water in the manual delineation, since both appear in black. In this case, the algorithm delineated the shoreline better.

Overall, the automated shoreline delineation showed quality and accuracy enough to perform the historical progradation/erosion analysis of the Delta, especially due to the detection of almost any single terrain detail, which sometimes passes unnoticed to the delineator, when the delineation is handmade.

4.3 Handmade shoreline delineation

We delineated by hand the shoreline of five Landsat images downloaded from the USGS Earth Explorer (1986, 1992, 2002, 2011 and 2019, path 10, row 54), using ArcGis Software tools for digitation. We carefully draw the polyline from the Tarena zone in the Northwest to the Southwest in the sector of Marirrio Bay towards Bahía Colombia for each year. Then, we sequentially overlapped the shoreline delineations and compared the lost and gained areas, delineating a series of polygons for erosion and progradation. Finally, we used the ArcGis tool to calculate geometry and obtain the areas in km² and ha.

These calculations yielded a total erosion area of 9.40 km² and a total progradation area of 15.742 km² over 33 years. Values differ in some km² in comparison with those obtained with the GEE algorithm. We consider the manual delineation suitable, but the expert could ignore details that GEE is capable to detect. However, the tendency for both methods remains the same, demonstrating that progradation is the dominated morphological phenomena in the delta.

4.4 Automatic tracking of the Delta's shoreline erosion/progradation

We overlapped the composites of different years between 1985 and 2019 to determine changes in the shoreline of all outflows of the Atrato River Delta by measuring how much area (in pixels) gains due to progradation or loses due to erosion.

4.5 Erosion/progradation processes

The Atrato is a “bird foot type” delta, this type of deltas are river-dominated with a slight deviation to wave dominated (Qi *et al.*, 2016; Post, 2011; Galloway, 1975). Therefore, the river attributes (course, flow, sediment load, etc.) have a predominant impact in the Delta’s evolution.

We observed several erosion and progradation hotspots along the shoreline, even far of the delta outflows. In Figure 12, we point out those hotspots. The most active erosion processes occurred at Leoncito, Burrera and Tarena outflows, being the latter the one that underwent the largest erosion process between 1986 and 2019.

The outflows with notable progradation processes were El Roto, Pavas, Matuntugo, Coquitos and Leoncito. El Roto progradation in particular is remarkable, considering its relatively recent formation between 1898 (Post, 2011) and 1930 (Nieto, 2004), evolving to become the main river outflow nowadays.

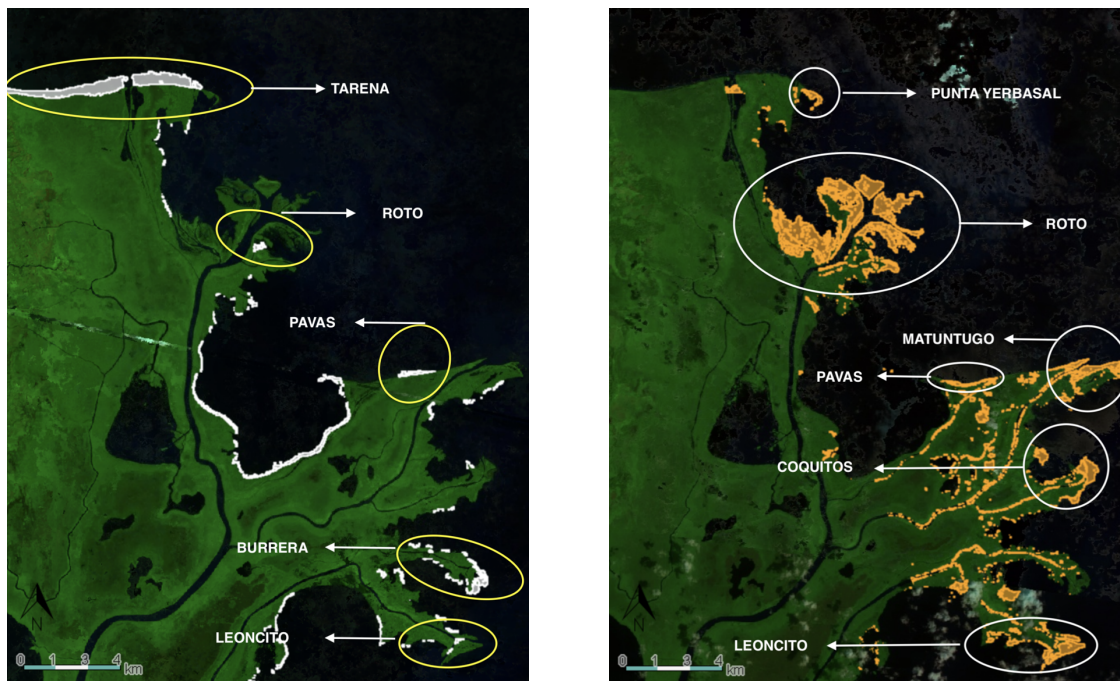


Figure 12. Coastal erosion (in white) and progradation (in orange) at Atrato River outflows in the period 1986 - 2019. Base image used for erosion was Landsat 8 2019 (left), base image used for progradation was Landsat 5 1986(right).

To determine the magnitude of erosion and progradation at the outflows, we took the polygons that represent them (Figure 12) and used the algorithm *area* in GEE to calculate the total coastal area loss/gain in 33 years.

4.5.1 Erosion

We found that the overall coastal area eroded during that period was 10.19 km² (1019 Ha). Figure 13 shows the magnitude of the erosion at the hotspots identified on each of the delta outflows.

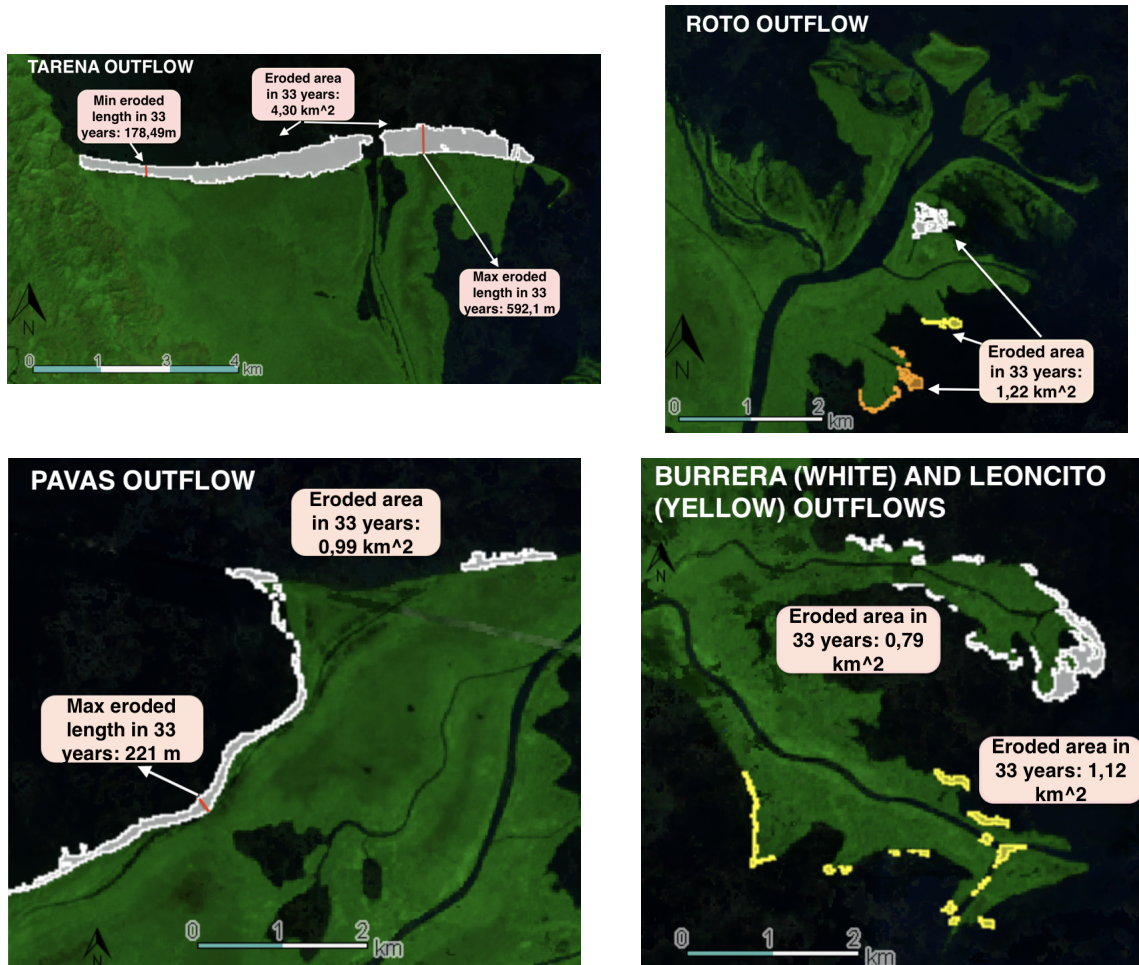


Figure 13. Eroded area at Atrato River outflows.

We calculated differential erosion rates per year (subtracting between two consecutive periods) and an “average” rate (subtracting the last period from the first one). Table 3 shows the values of eroded area and maximum eroded length for all Atrato River outflows as well as the average rates (we will discuss the differential rates in the next section).

Table 3. Erosion values at the Atrato River outflows.

OUTFLOWS	ERODED AREA (km ²)	EROSION RATE (km ² /yr)	MAX ERODED LENGTH (m)	EROSION RATE (m/yr)	MAGNITUDE
Tarena	4.30	0.13	-592.1	-17.94	High erosion
El Roto	1.22	0.037	-589.3	-17.86	High erosion
Pavas	0.90	0.027	-221.1	-6.70	High erosion
Burrera	0.79	0.024	-629.3	-19.07	High erosion
Leoncito	1.12	0.034	-163.7	-4.96	High erosion

The Tarena outflows presented the larger erosion process, accounting for 46.20% of the total area eroded between 1986-2019. The erosion at Tarena reached an area of 4.30 km² (432 Ha) in 33 years and the maximum eroded length of their shoreline was 592.1 m, with a mean shoreline recession of -17.94 m/yr (Table 3). According with the classification proposed by Rangel-Buitrago *et al.* (2015), Tarena outflows experienced high erosion (≥ -1.5 m/yr).

- **Tarena Landscape**

Tarena is an outflow located near the open sea, therefore its morphology is influenced by ocean waves that prone erosion (Post, 2011). Furthermore, since El Roto became the main outflow, much of the flow and sediments were diverted from Tarena, diminishing the contribution of sediment loads and favoring the notable process of erosion in this outflow (Nieto, 2004).

- **El Roto Landscape**

El Roto was the second outflow of marked erosion, with an area loss of 1.22 km² and a shoreline recession of -221.01 m between 1986-2019. The loss rate was -17.86 m/yr, which falls in the category of high erosion.

- **Pavas Leoncito and Burrera Landscape**

The Pavas outflow in turn is located near to open sea and is an abandoned delta branch, similar to Tarena. Therefore, given the river-dominance in the delta formation and the sediments decline, the outflow is prone to coastal erosion and shoreline recession. This is clear when we compared images from different periods. For instance, the water channel in Pavas widens between 2010 and 2019, indicating a tendency to reactivate the branch by connecting it to the river (Figure 15).

Burrera was the outflow with lower area lost to erosion, with 0.79 km². Pavas and Leoncito outflows presented values of 0.90 km² and 1.12 km² respectively.

Lost area and shoreline recession show different magnitudes, which means that, although Pavas was the second outflow with lost area, its shoreline recession value was the fifth between seven analyzed outflows. This is due to the shapes of the coastal erosion area: while Burrera has a rounded shape concentrated on one area (a portion of the lobe), the erosion on Pavas is parallel to the shoreline and spreads along a large area.

4.5.2 Progradation

We found great progradation processes in almost all delta outflows, except for Tarena. Unlike erosion, which distributes along all shorelines in the Delta, progradation is concentrated in the outflow zones. This pattern could be due to the direct accumulation of sediments in the confluence of ocean and fluvial currents that allow the deposition in the distal part of outflows, before the final deposition of suspended sediments in the Urabá Gulf.

- **El Roto Landscape**

Progradation was especially notable at El Roto outflow, which is currently the main outflow and therefore transports most of the river's flow and sediment. Although lower in magnitude but of important extension, Leoncito outflow presented also a remarkable area of progradation.

The total progradation area in all the shoreline around the Atrato Delta (including shorelines far from the outflows) was 17.68 km² (1768 ha). We selected the branches and its outflows where we found the main progradation processes to determine their behavior and to calculate the gained area (Figure 14 and Table 4).

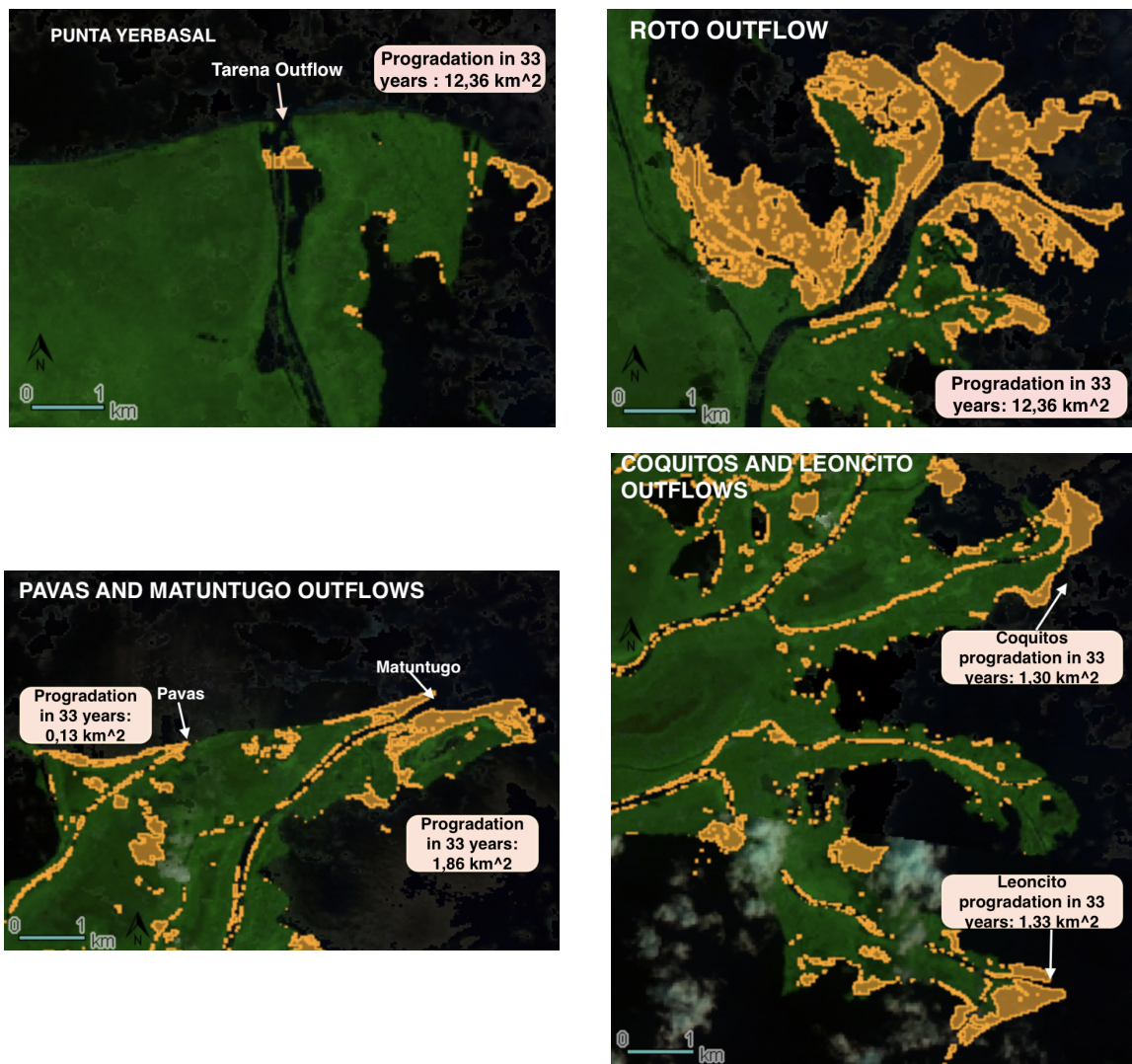


Figure 14. progradation hotspots at Atrato River outflows.

Table 4. Progradation values at Atrato River outflows.

OUTFLOWS	ACCRETED AREA (km ²)	ACCRETION RATE (km ² /yr)
Punta Yerbasal (near to Tarena outflow)	0.43	0.013
El Roto	12.36	0.37
Pavas	0.13	0.004
Leoncito	1.33	0.04
Matuntugo	1.86	0.056

- **Punta Yerbasal Landscape**

Punta Yerbasal is a relatively recent formation (in 1986 it was barely noticed). Nieto (2004) reported that the formation of Punta Yerbasal was a consequence of the Tarena outflow progressive deactivation and consequent coastal erosion. The material coming from the erosion in Tarena helped to create a coastal spike named Punta Yerbasal that, by 1990, had a length of 650 m (Nieto, 2004). We found that by 2019 this length had a maximum value of 1084 m with a progradation rate of 32.8 m/yr.

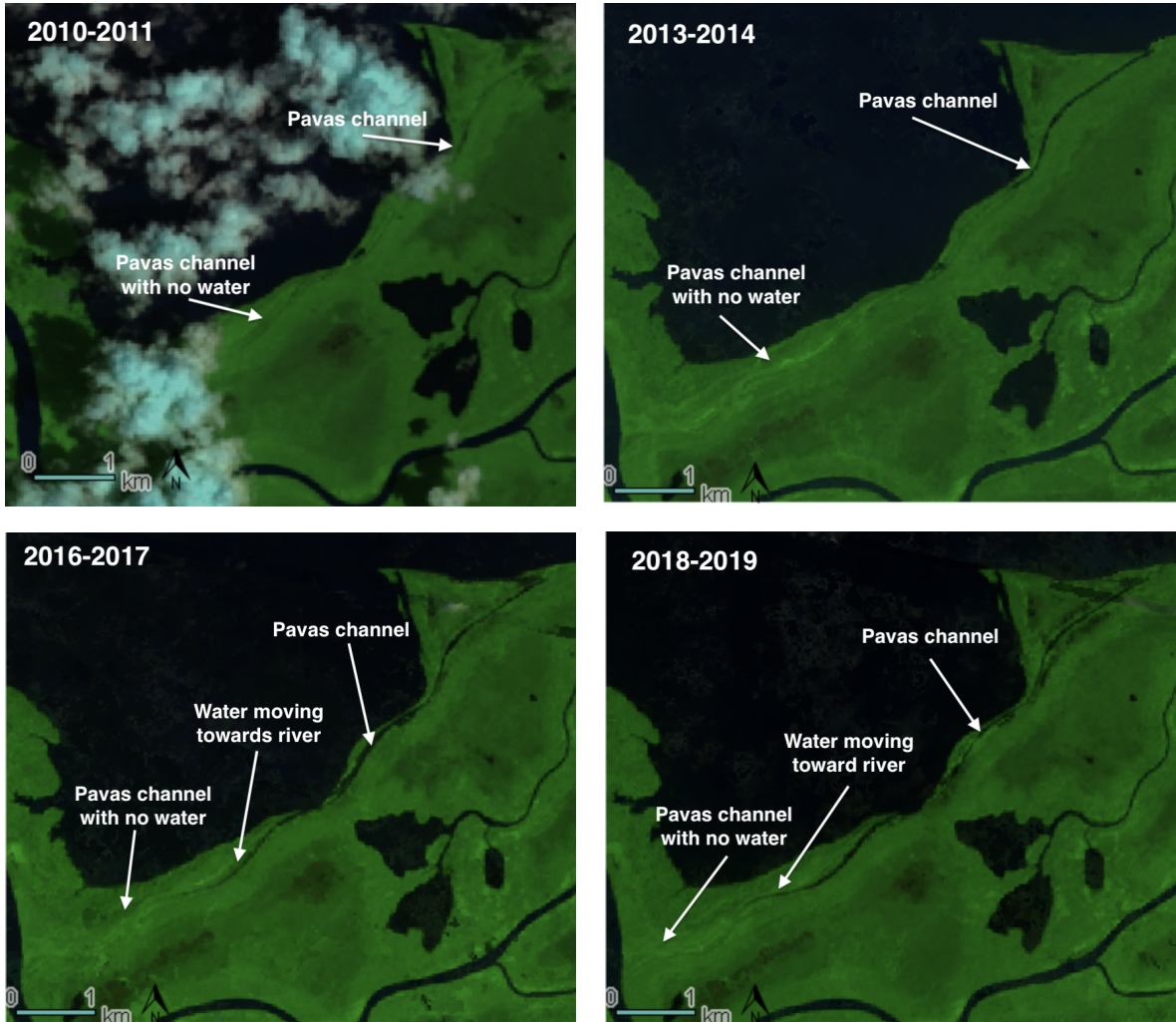
At present, El Roto is the main river branch, which created a small bird-foot delta (Nieto, 2004). El Roto branch is divided into several outflow channels, which together presented a total progradation area of 12.36 km². This exceeds the overall area lost due to erosion.

Progradation at El Roto outflow is not uniform, but forms islands and spikes around the main channel, with progradation lengths that vary from 1837 m in its northwestern part to 4841 m in its central part. The formation of these islands and spikes occurred around 1989.

- **Pavas and Matuntugo Landscape**

At Pavas and Matuntugo outflows, the progradation was small (0.13 km² and 1.86 km² respectively). Despite its proximity, Matuntugo outflow shows larger progradation than Pavas, which presented larger areas of erosion than progradation. This could be because, some years before 2010, the channel Pavas was disconnected from the river (Figure 15), losing its sediments loads.

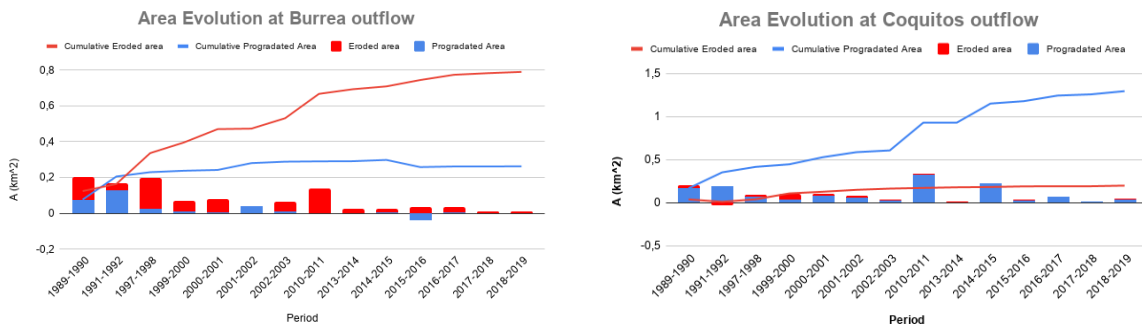
From the Landsat image of 1973, showed that Pavas outflow was active and feeded from the main Atrato channel and did not have direct output to the Candelaria Bay. The closing of Pavas occurred sometime between 2001 and 2011 (based in Landsat images 1996, 2001 and 2011) and the evidences in field exhibit sediments accumulation and plants grown as a kind of natural plug. From 2011, the active erosion in Candelaria Bay rised Pavas channel and connected this outflow with the sea. Last images dating from 2018 and 2019 reveals a new possible activation of this channel, mainly in the East side, but feeding for seawater.



Source: Own elaboration, 2019
 Figure 15. Evolution of Pavas branch, the water is moving through the dry channel towards the river

4.5.3 Annual and cumulative erosion/progradation

Figure 16 shows the Pareto charts of annual and cumulative values of erosion/progradation for each delta outflow and its vicinities. Cumulative values (red/blue lines for erosion/progradation) allow to watch trends in the evolution of the outflows, while annual values (red/blue bars for erosion/progradation) allow to explore changes in a particular year.



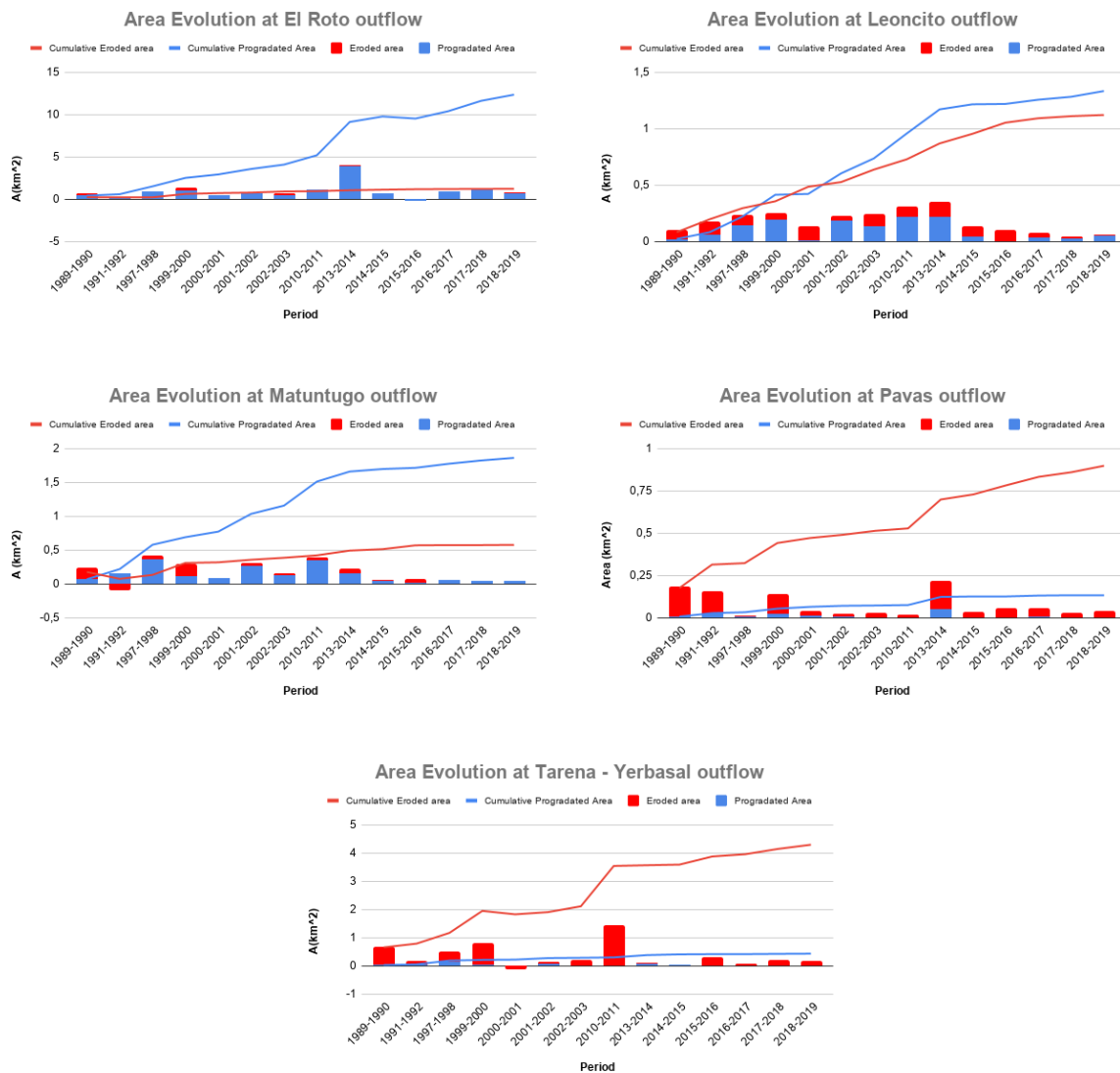


Figure 16. Area evolution at delta outflows. Erosion in red, progradation in blue.

In almost all delta outflows we found a dominant process, except for the Leoncito outflow that presents even erosion and progradation. Erosion at Leoncito spreads slightly over its shorelines, whereas progradation concentrates in specific areas, such as the delta's mouths and spikes (Figure 12).

Progradation is the dominant process in Coquitos, Roto and Matuntugo outflows whereas erosion is the dominant process in Burrera, Pavas and Tarena-Yerbasal. Except Tarena-Yerbasal, almost all of the progradation process concentrates in the area where the river branches meet the ocean, which is consistent with the definition of the Atrato River delta as a river-dominant delta.

Progradation at Tarena-Yerbasal occurs east of the Tarena outflow, in a spike named Punta Yerbasal. This spike formed around 1960, fostered by sediments carried from the progressive deactivation and erosion of the Tarena outflow (Nieto, 2004).

In 1997-1998, 1999-2000 and 2010-2011, 2013-2014 all delta outflows experienced a remarkable change in the tendency of their dominant processes, showing steeper slopes.

These changes coincide with strong La Niña events occurred between 1998-1999 and 2010-2011, which could explain the observed accelerations. Although less evident, the same happened in 1989-1990, which coincided with another La Niña event in 1988-1989 (NOAA, 2019).

On the other hand, Burrera, El Roto and Matuntugo outflows presented negative values in particular periods. In El Roto, for instance, this change implied that some features that appeared in 2013-2014 disappeared afterwards in 2015-2016.

According to Figure 16, all non-dominant processes have a tendency to stabilize after 2013-2014, except for the Leoncito outflow that shows this tendency after 2015-2016. Nonetheless, the dominant processes did not show this tendency. Although the slope of the cumulative line decreased after the same periods, these lines showed a constant growth.

The change in slope of the cumulative lines indicate that both dominant and non-dominant processes respond to particular climate events (i.e., La Niña years), although dominant processes may also respond to additional forcings that drive the continuity of the process (i.e., land cover changes at the Atrato River basin and hydrodynamics of the Gulf of Urabá).

Figure 17 shows the most representative outflows in erosion and progradation processes, the Tarena-Yerbasal and El Roto respectively. In this figure, we observe that 2013-2014 was the period with the larger progradation, and 2010-2011 the period with the larger erosion process to date.

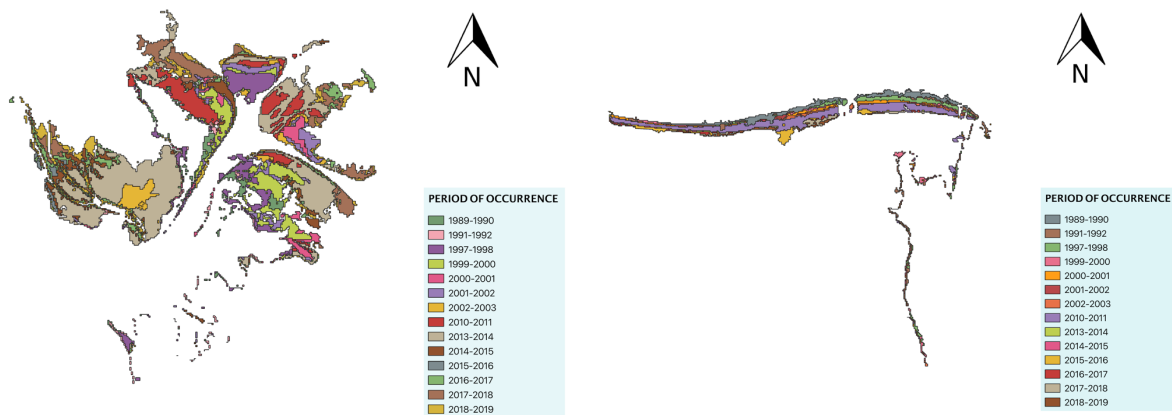


Figure 17. Progradation evolution at El Roto (left) and erosion evolution at Tarena-Yerbasal (right) delta outflows

In Figure 18 we summarize the overall erosion and progradation between 1986 and 2019, as we obtain them from our algorithm (left image), and delineated by hand (right image). The results in both images are similar, although the delineation by hand shows less detailed polygons in some places, where clouds may have hindered the real shoreline.

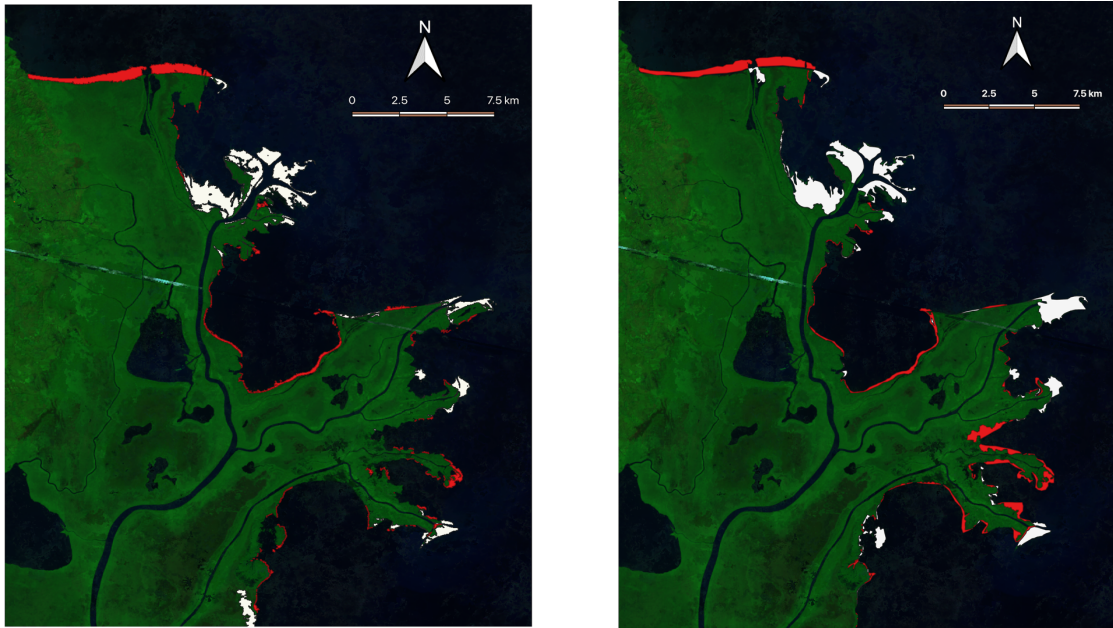


Figure 18. Erosion (in red) and progradation (in white) processes along the Atrato delta. Left image: automated delineation; Right image: handmade delineation.

4.6 Possible causes of the progradation and erosion fronts

There is controversy over the origin of progradation of the Atrato in the Western side of the gulf. Some authors claim slow growth, compared to other smaller deltas present in the Eastern side and the ocean drift that does not allow the distribution of sediments of the Atrato along the Gulf (Thomas *et al.*, 2007; Nieto, 2004; Robertson & Martínez, 1999). These claims are supported in historical cartographic reviews of satellite images and ancient maps dating from 1817 to 1846 (IGAC, 1985), which show a relative stability of this landform over the past 170 years. The most significant change is the replacement of the influx of Tarena mouth by the direct river outflow to the sea in El Roto, which is not visible on the old maps.

There is also a remarkable coastal erosive trend in the drainage catchments of the Atrato River, supported by higher rates of sedimentation towards the northeast of the Gulf and not towards the proximal area of the delta (Velez & Aguirre, 2016).

An evidence of the structural control of the gulf is the elongated geometry of 80 km in length, 25 km in width and depths of 30 m, measured by bathymetric studies and possibly limited by a fault system in both sides of the gulf (Thomas *et al.*, 2007; Robertson & Martínez, 1999). The Atrato Delta could relate to a phenomenon of subsidence of sedimentary sequences to the West (Chevillot & Giraldo, 1993). In addition, in terms of tectonics, there could be a process of "sinking" possibly due to the deposits of river and marine muddy sediments. Both situations incorporate a low probability to the future closure of the Gulf, due to the sedimentation caused by the Atrato Delta (Robertson & Martínez, 1999).

Nevertheless, hydrodynamic studies support the significant effect of the Atrato Delta on the Gulf of Urabá. These studies discuss the importance of the Atrato River in terms of its sediment loads to the system, from Bahía Colombia towards the North, almost to the open

sea, and its influence in the reduction of the currents' kinetic energy toward the northwest (Escobar, 2011).

Additionally, grain size studies of surface sediments determined the presence of sand deposits in front of the delta mouths (Alvarez & Bernal, 2007), an aspect that confirms the relative occurrence of the progradation, but not necessarily support these coarse sediments come from the delta flow and could be more related with marine sediments contributions. However, the North-South direction of sediment transport casts doubt on the constant sediment deposit in this sector of the delta.

A crosscutting factor for the development of the delta is the 2400-year sea level decline that has favored progradation in the northeast direction and has possibly increased over the past 200 years AP, with the growth of anthropic activities related to logging and mining (Agudelo & Aguirre, 2016).

Mining is another factor that may influence sedimentation rates in the delta. Gold mining is an important economic activity in the Atrato River basin. This activity had a peak in gold production between years 2010-2012 (UPME, 2017). In figure 19, we compare progradation areas with mining production in the Atrato River basin.



Figure 19. Relationship between gold mining production and prograded areas.

Dredgers perform mining activities in the river and produce large amounts of sediments. Therefore, a rise in gold production would likely increase sediment loads and progradation areas. In any given year, we measured progradation from November to April whereas gold production records go from January to December. Therefore, in Figure 19 we can assume a relative lag of approximately one year between coincident peaks in mining production and progradation at Coquitos, Leoncito and Matuntugo mouths, whereas in El Roto mouth (which is the main mouth and thus has the longest branch) the lag is of two years. The peak of mining

production matches also with La Niña years, which could further exacerbate sediment production and transport.

5. CONCLUSIONS

The shoreline delineations that we obtained with our algorithm in GEE were satisfactory, performing even better than the delineations drawn by an expert in higher resolution images, particularly when defining areas such as islands and segments affected by some haze or the area with small size, difficult to detect by eye. The results improve when more images are available, especially in regions with high cloudiness and haze year round. Nonetheless, verification is always important, since the presence of “noise” in the images (caused by high contrasts due to cloud shadows, for instance) may mislead the automatic delineation of the algorithm. This implies additional manual processing to clean the image in external softwares and eventually the discarding of the image composite.

We tracked the Atrato Delta’s evolution using the algorithm, and the results are consistent with the expectations from a bird-foot delta, with an especial fluvial domain: on the one hand, progradation is the overall dominant process in the Delta’s mouths, where branched rivers reach the ocean with large sediment loads. Only two outflows out of seven (Tarena and Pavas) exhibit erosion as the dominant process in their mouths. On the other hand, erosion is the dominant process along the shorelines, far from the delta outflows, where the ocean hydrodynamics is more relevant than the riverine factors.

Tarena and Pavas outflows experienced erosion instead of progradation since both are branches with river disconnection processes. Tarena used to be the main branch but this changed with the consolidation of El Roto delta flow in the last century, which decreased Tarena’s flows and sediment loads, leading to the dominance of ocean dynamics in this outflow.

Pavas experienced a total disconnection from the Atrato River, which also explains why erosion is its dominant process. However, our analysis suggests that this branch is in a current process of reconnection, advancing from the ocean to the river (field data will be necessary to confirm and determine the causes of this trend), possibly related with an upcoming rise period of sea level.

Using the progradation and erosion areas calculated with GEE, we conclude that progradation is the dominant process at the Atrato Delta, with a total area of 17.68 km², while erosion encompasses only 10.19 km². Nevertheless, certain outflows presented erosion as their local dominant process, but more related with the decrease of river energy flow that has given way to control of marine phenomena associated with tides and currents that promote the erosion.

The values of progradation and erosion obtained with the automated process and handmade differ in a few km². The automated process shows higher values than handmade, for erosion process the difference was 0.79 km² and for progradation 1.93 km². This difference could be due to the capacity of the algorithm to detect details that the expert may not notice.

When erosion or progradation are dominant, they seem to keep a growing trend along the years. However, when they are not dominant, they tend to stabilize or to switch. In certain periods, likely related to La Niña years, the trends accelerate. However, more research is

necessary to establish a sound correlation between extreme events and the accelerated rates of erosion and progradation.

The increasing trends of dominant processes highlights the active nature of sediment loads in this delta. In this regard, the next stage is to investigate how other factors (i.e., tectonics, sea level oscillation, land cover changes at the Atrato River basin, the hydrodynamics of the Gulf of Urabá, the geomorphology of the delta, human interventions and climate change) affect these trends. In this regard, for instance, mining activities partially induce progradation in the Atrato delta, by increasing sediment loads in specific years (i.e., 2010-2012). Although we identify such influence, the result is not conclusive. Future studies could focus on investigating the relationship between mining and land cover changes in general, and the increased progradation of the delta.

The trends are consistent with academic works developed in the same area by Rangel-Buitrago *et al.* (2015), Nieto (2004), Bernal *et al.* (2005) and Post (2011). These studies used cartography, satellite imagery and field validation and showed the same trends as we do now in our research. Hence, we are confident that our algorithm is an efficient tool to track shoreline erosion/progradation processes. Furthermore, the algorithm is suitable for areas with limited access to field data and computational resources.

The accuracy of the automated delineation depends on the image cleanliness, i.e. low cloudiness and contrast homogeneity. One option to improve the results is by using SAR (Synthetic Aperture Radar) images that may be taken at any time (day or night), regardless of cloud coverage. The Sentinel-1 mission provides scenes in one of three resolutions (10, 25 or 40 meters) and is free to use in GEE. However, we did not use them in this study due the short period of data available (from 2014 up to today). Nevertheless, it is a good alternative when performing short-term analysis or in the future, when Sentinel-1 mission has longer records.

It could be helpful to use Digital Elevation Models (DEM) as ancillary data in future studies, mainly to correct delineation by using slope and elevation. However, DEM results in very flat areas (like the subaerial Atrato River delta), must be used with caution, due to its few elevation differences and hence, its low slopes.

Otsu method is one of many methods for image segmentation that is simple to use. Nonetheless, other methods could be more efficient and faster, like the Convolutional Neural Networks (CNN) and its variations (edge detection, Conditional Random Field (CRF), among others). Future studies could test the performance and accuracy of these methods, compared to schemes that are more sophisticated.

Finally, the algorithm that we developed is suited for any delta or coastline in which we are interested in gathering insights about erosion and progradation processes (it would only require a change of coordinates and a delineation of a new polygon of the region of interest). Further improvements to the algorithm would include a GUI application that only require the user to draw a polygon of the region of interest for the algorithm to show the results, maps and charts automatically.

6. REFERENCES

- Álvarez, A. M., & Bernal, G. (2007). Estimación del campo de transporte neto de sedimentos en el fondo de Bahía Colombia con base en análisis de tendencia del tamaño de grano. *Avances En Recursos Hidráulicos*, (16), 41–50.
- Abbott, S., Julian, J., Kamarinas, I., Meitzen, K.M., Fuller, I., McColl, S.T. & Dymond, J.R. (2017). State-Shifting at the edge of resilience: River suspended sediment responses to land use change and extreme storms. *Geomorphology*, 305. 49-60. <https://doi.org/10.1016/j.geomorph.2017.09.004>.
- Alonso, A., Muñoz-Carpena, R., Kennedy, R.E. & Murcia, C. (2016). Wetland landscape spatio-temporal degradation dynamics using the new Google Earth Engine cloud-based platform: opportunities for non-specialists in remote sensing. *Wetlands & Coastal Systems*, 59(5). 1333-1344. doi: 10.13031/trans.59.11608.
- Amorosi, A. & Milli S. (2001). Late quaternary depositional architecture of Po and Tevere River deltas (Italy) and worldwide comparison with coeval deltaic successions. *Sedimentary Geology*, 144. 357-375. [https://doi.org/10.1016/S0037-0738\(01\)00129-4](https://doi.org/10.1016/S0037-0738(01)00129-4)
- Arroyave-Rincón, A., Blanco, J.F. & Taborda, A. (2012). Exportación de sedimentos desde cuencas hidrográficas de la vertiente oriental del Golfo de Urabá: Influencias climáticas y antrópicas. *Revista Ingenierías Universidad de Medellín*, 11(20). 13-30.
- Bao, S. & Chung, A. (2018). Multi-scale structured CNN with label consistency for brain MR image segmentation. *Computer methods in biomechanics and biomedical engineering: Imaging & visualization* 6(1). 113-117. <https://doi.org/10.1080/21681163.2016.1182072>
- Bernal, G., Montoya, L., Garizábal, C. & Toro, M. (2005). La complejidad de la dimensión física en la problemática costera del golfo de Urabá, Colombia. *Gestión y Ambientel*, 8(1). 123-135.
- Blanco-Libreros, J. F. (2016). Cambios globales en los manglares del golfo de Urabá (Colombia): entre la cambiante línea costera y la frontera agropecuaria en expansión. *Actualidades Biológicas*, 38(104), 53–70. <https://doi.org/10.17533/udea.acbi.v38n104a06>
- Blanco-Libreros, J.F., Taborda-Marín, A., Amortegui-Torres, V., Arroyave-Rincón, A., Sandoval, A., Estrada, E.A., Leal-Flórez, J., Vásquez, J.G. & Vivas, A. (2013). Deforestación y sedimentación en los manglares del Golfo de Urabá. *Gestión y Ambiente*, 16(2). 19-36.
- Boyd, R., Dalrymple, R. & Zaitlin, B. (1992). Classification of clastic coastal depositional environments. *Geology*, 17. 926-929. [https://doi.org/10.1016/0037-0738\(92\)90037-R](https://doi.org/10.1016/0037-0738(92)90037-R)
- Buynevich, I., Jol, H. & FitzGerald, D. (2009). Coastal environments. In Jol, H.M. (Ed.). *Ground penetrating radat theory and applications*. Elsevier Science. Amsterdam.
- Catuneanu, O. (2002). Sequence stratigraphy of clastic systems: concepts, merits and pitfalls. *Journal of African Earth sciences*. 35(1). 1-43. [https://doi.org/10.1016/S0899-5362\(02\)00004-0](https://doi.org/10.1016/S0899-5362(02)00004-0)

Cuesta, T. & Ramírez, G. (2009). Evaluación interdimensional de impactos ambientales sobre la dimensión física ocasionados por cultivos de palma aceitera y la ganadería extensiva en la selva húmeda tropical del Bajo Atrato. *Gestión y Ambiente*, 12(3). 37-48.

Chen, L., Barron, J., Papandreou, G., Murphy, K. & Yuille, A. (2016). Semantic image segmentation with task-specific edge detection using CNNs and a discriminatively trained domain transform. *Computer vision foundation*. Work done in part during internship at Google Inc.

Chevillot, Ph. Molina, A. Giraldo L. 1993. Estudio hidrológico y geológico del Golfo de Urabá. CIOH, BoL Cient. 14: 79-89.

Coleman, J. & Wright, L. (1975). Modern river deltas: Variability of processes and sand bodies. In Broussard, M.L. (Ed.) *Deltas: models for exploration*. Houston Geological Society. Houston. 99-149

Dalrymple, R., Zaitlin, B. & Boyd, R. (1992). Estuarine facies models; conceptual basis and stratigraphic implications. *Journal of Sedimentary Research* 62 (6). 1130-1146.

Dang T., Cochrane, T. & Arias, M. (2018). Quantifying suspended sediment dynamics in mega deltas using remote sensing data: A case study of the Mekong flood plains. *International journal of applied Earth observation and geoinformation*, 68. 105-115. DOI: 10.1016/j.jag.2018.02.008.

Díaz, J.M. (2007). Deltas y Estuarios del Caribe Colombiano. In J.M. Díaz Merlano, *Delta y Estuarios de Colombia*. Cali: Comité Editorial Banco de Occidente.

Dolozzi, M. B., Kalindekaffe, L. S. N., Ngongondo, C., & Dulanya, Z. (2011). A comparative analysis of the distribution, composition and geochemistry of surface sediments in the Linthipe and Songwe River Deltas of Lake Malawi. *Journal of African Earth Sciences*, 60(3), 93–105. <https://doi.org/10.1016/j.jafrearsci.2011.02.002>

Donchyts, G., Baart, F., Winsemius, H., Gorelick, N., Kwadijk, j. & Van de Giesen, N. (2016). Earth's surface water change over the past 30 years. *Nature Climate Change*, 6(9). 810-813. DOI: 10.1038/nclimate3111.

Elliot, T. (1986). Deltas. In H.G. Reading (Ed.). *Sedimentary Environments and Facies*, (pp. 113-154). Oxford, Blackwell Scientific.

Escobar, C. a. (2011). Relevancia de Procesos Costeros en la Hidrodinámica del Golfo de Urabá (Caribe Colombiano). *Boletín de Investigaciones Marinas y Costeras*, 40(2), 327–346. <http://hdl.handle.net/1834/4510>.

Escobar, C. A., Velázquez, L. & Posada, F. (2015). Marine Currents in the Gulf of Urabá, Colombian Caribbean Sea. *Journal of Coastal Research*, 1363–1375. <https://doi.org/10.2112/JCOASTRES-D-14-00186.1>

Fan, Y., Chen, S., Zhao, B., Pan, S., Jiang, C., & Ji, H. (2018). Shoreline dynamics of the active Yellow River delta since the implementation of Water-Sediment Regulation Scheme:

A remote-sensing and statistics-based approach. *Estuarine, Coastal and Shelf Science*, 200. 406–419. DOI:10.1016/j.ecss.2017.11.035

Federal Emergency Management Agency (FEMA). (1997). Multi-hazard risk identification and assessment: A cornerstone of the National Mitigation Strategy, prepared in support of the International Decade for Natural Disaster Reduction. From: https://www.fema.gov/pdf/floodplain/is_9_complete.pdf

Galloway, W. E. (1975). Process Framework for Describing the Morphologic and Stratigraphic Evolution of Deltaic Depositional Systems. *Deltas: Models for explorations*. 87-98.

Google Inc. (2018). Google Earth Engine API, Accessed through https://developers.google.com/earth-engine/tutorial_api_06. (17-04-2018)

Gorelick, N., Hancher, M., Dixon, M., Ilyushchenko, S., Thau, D. & Moore, R. (2017). Google Earth Engine: Planetary-scale geospatial analysis for everyone. *Remote Sensing of Environment*, 202. 18-27. <https://doi.org/10.1016/j.rse.2017.06.031>.

Haddow, G., Bullock, J. & Coppola, D. (2017). Natural and technological hazards and risk assessment. In *Introduction to emergency management (6 edition)*. Oxford. 33-77

Hakkou, M., Maanan, M., Belrhaba, T., El khalidi, K., El Ouai, D., & Benmohammadi, A. (2018). Multi-decadal assessment of shoreline changes using geospatial tools and automatic computation in Kenitra coast, Morocco. *Ocean & Coastal Management*, 163. 232–239. DOI: 10.1016/j.ocecoaman.2018.07.003

Hori, K. & Saito Y. (2007). Classification, architecture, and evolution of large-river deltas. In A. Gupta (Ed.). *Large Rivers: Geomorphology and Management*, (pp. 75-96). John Wiley & Sons, Ltd.

IDEAM, (2018). Instituto de Hidrología, Meteorología y Estudios Ambientales. From: <http://www.ideam.gov.co/>

IGAC, (1985). Instituto Geográfico Agustín Codazzi. From: <https://www.igac.gov.co/>

Institute for Water Resources (IWR). (2011). Coastal storm risk management, IWR report. U.S. Army Engineers for Water Resources.

Islam, T. & Ryan, J. (2016). Hazard identification - Natural Hazards. In Haddow, G., Bullock, J. & Coppola, D. (Ed.). *Hazard mitigation in emergency management*. Oxford. 129-170.

Jayakumar, K. & Malarvannan, S. (2016). Assessment of shoreline changes over the Northern Tamil Nadu Coast, South India using WebGIS techniques. *Journal of coastal conservation*, 20(6). 477-487. <https://doi.org/10.1007/s11852-016-0461-9>

Jerolmack, D. (2009). Conceptual framework for assessing the response of delta channel networks to Holocene sea level rise. *Quaternary science reviews*, 28(17). 1786-1800. <https://doi.org/10.1016/j.quascirev.2009.02.015>

Kaliraj, S., Chandrasekar, N. & Magesh, N. (2013). Evaluation of coastal erosion and accretion processes along the southwest coast of Kanyakumari, Tamil Nadu using geospatial techniques. *Arabian Journal of Geosciences*, 8, 239-253. <https://doi.org/10.1007/s12517-013-1216-7>

Kröger, R., Moore, M. T., Locke, M. A., Cullum, R. F., Steinriede, R. W., Testa, S., Cooper, C. M. (2009). Evaluating the influence of wetland vegetation on chemical residence time in Mississippi Delta drainage ditches. *Agricultural Water Management*, 96(7), 1175–1179. <https://doi.org/10.1016/j.agwat.2009.03.002>

Kubo, Y., Syvitski, J. & Hutton, E. (2006). Inverse modeling of post Glacial Maximum transgressive sedimentation using 2D-SedFlux: Application to the northern Adriatic sea. *Marine Geology*, 234, 233-243. <https://doi.org/10.1016/j.margeo.2006.09.011>

Kuenzer, C., Klein, I., Ullmann, T., Georgiou, E. F., Baumhauer, R., & Dech, S. (2015). Remote Sensing of River Delta Inundation: Exploiting the Potential of Coarse Spatial Resolution, Temporally-Dense MODIS Time Series. *Remote Sensing*, 7(7), 8516–8542. Doi: 10.3390/rs70708516.

Li, X., Liu, J. P., Saito, Y., & Nguyen, V. L. (2017). Recent evolution of the Mekong Delta and the impacts of dams. *Earth-Science Reviews*, 175, 1–17. <https://doi.org/10.1016/j.earscirev.2017.10.008>

Libreros, J. F. B., Mesa, M. H. L., Arango, I. D. C., Arias, A. F. O., Franco, G. R. B., Vorenberg, J. H. P., & Giraldo, L. E. U. (2013). Crónicas de la Expedición Exploración del Golfo de Urabá 2007-2013, 31.

Liu, F., Lin, G. & Shen, C. (2015). CRF learning with CNN features for image segmentation. *Pattern recognition* 48(10). 2983-2992. <https://doi.org/10.1016/j.patcog.2015.04.019>

Longhitano, S. & Colella, A. (2007). Geomorphology, sedimentology and recent evolution of the anthropogenically modified Simeto River delta system (eastern Sicily, Italy). *Sedimentary Geology*, 194(3–4), 195–221. <https://doi.org/10.1016/j.sedgeo.2006.06.004>

Maselli, V., Trincardi, F., Asioli, A., Ceregato, A., Rizzetto, F., & Taviani, M. (2014). Delta growth and river valleys: The influence of climate and sea level changes on the South Adriatic shelf (Mediterranean Sea). *Quaternary Science Reviews*, 99, 146–163. <https://doi.org/10.1016/j.quascirev.2014.06.014>

Mateos-Molina, D., Palma, M., Ruiz-Valentín, I., Panagos, P., García-Charton, J.A. & Ponti, M. (2015). Assessing consequences of land cover changes on sediment deliveries to coastal waters at regional level over the last two decades in the northwestern Mediterranean Sea. *Ocean & Coastal Management*, 116, 435-442. <http://dx.doi.org/10.1016/j.ocecoaman.2015.09.003>.

Meyer, H. & Nijhuis, S. (2013). Delta urbanism: planning and design in urbanized deltas – comparing the Dutch delta with the Mississippi River delta. *Journal of Urbanism*, 6(2), 160–191. DOI: 10.1080/17549175.2013.820210

Mikhailova, M.V. (2014). Morphometry of river deltas. *Water resources*, 42(1). 45-55. DOI: 10.1134/S009780781501008X

Millerati, F., Navab, N. & Ahmadi, S. (2016). V-net: Fully convolutional neural networks for volumetric medical image segmentation. *Fourth international conference on 3D vision*. DOI: 10.1109/3DV.2016.79.

Morita, A., Shouji, T., Kuwae, T., Nishimura, O. & Sakamaki, T. (2017). Effects of watershed land-cover on the biogeochemical properties of estuarine tidal flat sediments: A test in a densely-populated subtropical island. *Estuarine, Coastal and Shelf Science*, 184. 207-213. <https://doi.org/10.1016/j.ecss.2016.11.019>.

Nadipally, M. (2019). Optimization of methods for Image-Texture segmentation using ant colony optimization. *Intelligent data analysis for biomedical applications*. Elsevier Inc. 1-27. <https://doi.org/10.1016/B978-0-12-815553-0.00002-1>

Nemec, W. (1990). Deltas: Remarks on terminology and classification. In Colella, A. and Prior, D.B. (Eds.) *Coarse grained deltas. International Association of Sedimentologist, Special publication 10*. Oxford. 3-12.

Nieto, M.J. (2004). Estudio morfodinámico del delta del río Atrato, golfo de Urabá, a partir de cartografía histórica y percepción remota (Trabajo de Grado para optar al título de Geólogo). Universidad Nacional de Colombia, Facultad de Ciencias, departamento de Geociencias. Colombia

NOAA (2019). National Oceanic and Atmospheric Administration. From: https://origin.cpc.ncep.noaa.gov/products/analysis_monitoring/ensostuff/ONI_v5.php. United States of America.

Otsu, N. (1979). A Threshold Selection Method from Gray-Level Histograms. *IEEE Transactions on Systems, Man, and Cybernetics*, 9(1). 62-66. DOI: 10.1109/TSMC.1979.4310076.

Overeem, I., Syvitski, J. & Hutton, E. (2005). Three-dimensional numerical modelling of deltas. In (L. Giosan & J.P. Bhattacharya, Eds.) *River deltas: concepts, models and examples*, 83. 13-30.

Parra, A. & Restrepo, J.D. (2014). El colapso ambiental en el río Patía, Colombia: variaciones morfológicas y alteraciones en los ecosistemas de manglar. *Latin American Journal of Aquatic Research*, 42(1). 40-60. DOI: 103856/vol42-issue1-fulltext-4.

Posada Posada, B. O., & Henao Pineda, W. (2008). Diagnóstico de la erosión en la zona costera del Caribe colombiano. INVEMAR, Serie Publicaciones Especiales, 13, 200.

Post, S. (2011). Morphological modelling of the Atrato River delta in Colombia (Master of science Thesis report). Delft University of Technology, Faculty of Civil Engineering and Geosciences. Holland.

Qi, M., Shun, Z., Guoxin, S., Xiuli, F., Chao, W., & Yao, S. (2016). A seismic geomorphology study of the fluvial and lacustrine-delta facies of the Cretaceous Quantou-

Nenjiang Formations in Songliao. *Marine and Petroleum Geology*, 78, 836–847. <https://doi.org/10.1016/j.marpetgeo.2016.01.017>

Rangel-Buitrago, N.G., Anfuso, G. & Williams, A.T. (2015). Coastal erosion along the Caribbean coast of Colombia: Magnitudes, causes and management. *Ocean & Coastal Management*, 114. 129-144. <http://dx.doi.org/10.1016/j.ocecoaman.2015.06.024>.

Renaud, F., Syvitski, J., Sebesvari, Z., Werners, S., Kremer, H., Kuenzer, C., Ramesh, R., Jeuken & A., Friedrich, J. (2013). Tipping from the Holocene to the Anthropocene: How threatened are major world deltas?. *Current Opinion in Environmental Sustainability*, 5(6). 644-654. <https://doi.org/10.1016/j.cosust.2013.11.007>.

Restrepo, J.D. (2008). Deltas: Visión general y procesos morfodinámicos. In Restrepo, J.D (Eds.). *Deltas de Colombia: Morfodinámica y vulnerabilidad ante el cambio global*, (pp. 27-50). Colombia: Fondo Editorial de la Universidad Eafit.

Restrepo, J.D. & Alvarado E. (2011). Assessing Major Environmental Issues in the Caribbean and Pacific Coast of Colombia, South America: An Overview of Fluvial Fluxes, Coral Reef Degradation and Mangrove Ecosystems Impacted by River Diversion. In *Treatise on Estuarine and Coastal Science* (pp. 289-314). Londres: Elsevier.

Restrepo, J.D. & Kjerfve, B. (2004). The Pacific and Caribbean Rivers of Colombia: Water Discharge, Sediment Transport and Dissolved Loads. In L. Drude, R. Erthal, E. Duursma & J. Abrao (Eds.). *Environmental Geochemistry in Tropical and Subtropical Environments* (pp. 169-185). New York: Springer-Verlag Berlin Heidelberg.

Restrepo, J.D. & López, S. (2008). Morphodynamics of the Pacific and Caribbean deltas of Colombia, South America. *Journal of South American Sciences*, 25(1). 1-21. <https://doi.org/10.1016/j.jsames.2007.09.002>.

Restrepo, J.D. & Restrepo, J.C. (2005). Efectos naturales y antrópicos en la producción de sedimentos de la cuenca del río Magdalena. *Revista Académica Colombiana de Ciencias*, 29(11). 239-254.

Robertson, K., & Martínez, N. (1999). Cambios del nivel del mar durante el holoceno en el litoral caribe colombiano. *Cuadernos de Geografía: Revista Colombiana de Geografía*, 8(1), 168–198.

Skaggs, L., & McDonalds, F. (1991). National economic development procedures manual: Coastal storm damage and erosion. U.S. Army Corps of Engineers.

Suter, J. (1994). Deltaic coasts. In R.W.G Carter & C.D. Woodroffe (Eds.) *Coastal evolution: Late quaternary shoreline morphodynamics*. Cambridge University Press. 87-120.

Syvitski, J. & Kettner, A. (2018). Sediment flux and the Anthropocene. *Philosophical Transactions of the Royal Society*, 369. 957-975. <https://doi.org/10.1098/rsta.2010.0329>.

Syvitski, J. & Saito, Y. (2007). Morphodynamics of deltas under the influence of humans. *Global and planetary change*, 57. 261-282. <https://doi.org/10.1016/j.gloplacha.2006.12.001>

Thomas, Y., García Valencia, C., Cesaraccio, M., & Rojas, X. (2007). Atlas del golfo de Urabá: una mirada al Caribe de Antioquia y Chocó. Atlas del golfo de Urabá: una mirada al Caribe de Antioquia y Chocó.

Thomas, D. & Goudie, A. (Eds.)(2000). The Dictionary of Physical Geography, 3rd edition. Blackwell, Oxford.

UPME, U. (2017). Unidad de Planeación Minero Energético UPME. From: http://www.upme.gov.co/GeneradorConsultas/Consulta_Series.aspx?idModulo=4. Colombia.

USGS (2019). Landsat Satellite Missions. From: https://www.usgs.gov/land-resources/nli/landsat/landsat-satellite-missions?qt-science_support_page_related_con=2#qt-science_support_page_related_con. USA.

Vala, H. & Baxi, A. (2013). A review on Otsu image segmentation algorithm. *International journal of advanced research in computer engineering & technology* 2(2). 387-389.

Vallejo Toro, P. P., Vásquez Bedoya, L. F., Correa, I. D., Bernal Franco, G. R., Alcántara - Carrió, J., & Palacio Baena, J. A. (2016). Impact of terrestrial mining and intensive agriculture in pollution of estuarine surface sediments: Spatial distribution of trace metals in the Gulf of Urabá, Colombia. *Marine Pollution Bulletin*, 111(1–2), 311–320. <https://doi.org/10.1016/j.marpolbul.2016.06.093>

Vann, J. H., & Vannl, J. H. (1959). Landform-vegetation Relationships In the Atrato Delta, 5608. *Annals of the association of the American Geographer*, 49(4). 345-360. <https://doi.org/10.1111/j.1467-8306.1959.tb01621.x>

Vélez C., A. N. (2016). Influencia del río atrato en el golfo de urabá durante el holoceno tardío, mar caribe colombiano. *Boletín de Investigaciones Marinas y Costeras*, 45(1), 73–97.

Viaña-Borja, S. & Ortega-Sánchez, M. (2019). Automatic methodology to detect coastline from Landsat images with a new water index assessed on three different spanish mediterranean delta. *Remote sensing* 11(18). 1-43. DOI:10.3390/rs11182186

Vilariño, D., Brea, V. & Pardo, J. (1998). Discrete-time CNN for image segmentation by active contours. *Pattern recognition letters* 19. 721-734.

Wang, H. & Dong, Y. (2007). An improved image segmentation algorithm based on Otsu method. International symposium of photoelectronic detection and imaging. In Zhou L. (Ed.) *Related technologies and applications*, 6625. DOI: 10.1117/12.790781

Wright, L.D. (1982). Deltas. In M.L. Schwartz (Ed.) *The encyclopedia of beaches and coastal environments*. Hutchinson Ross Publishing Co. 358-369.

Wright, L.D. (1985). River deltas. In A.R. Davis (Ed.) *Coastal sedimentary environments*. Springer-Verlag, 1-76.

Xu, J. (2006). Land accretion of the Yellow River delta as influenced by drainage basin factors. *Geografiska annaler*. 88A(1). 31-41.

